nature nanotechnology

Article

https://doi.org/10.1038/s41565-023-01366-7

Proximal tubules eliminate endocytosed gold nanoparticles through an organelle-extrusion-mediated self-renewal mechanism

In the format provided by the authors and unedited

Proximal tubules eliminate endocytosed gold nanoparticles through an organelle-extrusion mediated self-renewal mechanism

Yingyu Huang, Mengxiao Yu* and Jie Zheng*

Department of Chemistry and Biochemistry, The University of Texas at Dallas, 800 W. Campbell Rd., Richardson, Texas 75080, USA

*e-mail: mengxiao.yu@utdallas.edu, jiezheng@utdallas.edu

Content

Supplementary Fig.3. Accumulation of (+)-AuNPs and (-)-AuNPs in blood, major organs, and tissue of normal mice at 24h post intravenous injection.

Supplementary Fig.4. Representative images of H&E-stained silver enhanced kidney tissue sections of normal mice showing distribution of (+)-AuNPs in the renal cortex at 24h post intravenous injection.

Supplementary Fig.5. Histological difference among proximal tubules, distal tubules and collecting ducts.

Supplementary Fig.6. Representative images of H&E-stained silver enhanced other renal compartments of normal mice including the glomerulus, the distal tubules, the Loop of Henle, and the collecting ducts at 24 h post intravenous injection of (-)-AuNPs and (+)-AuNPs.

Supplementary Fig.7. Representative images of H&E-stained silver enhanced kidney tissue sections of normal mice showing distribution of (-)-AuNPs in the kidneys at 24h post intravenous injection.

Supplementary Fig.8. Quantification of the area fraction of silver enhanced AuNPs in proximal tubules of normal mice.

Supplementary Fig.9. Effect of inhibiting clathrin-mediated endocytosis using chlorpromazine (CPZ) on the kidney accumulation, renal clearance efficiency and distribution in proximal tubules of (+)-AuNPs.

Supplementary Fig.10. Renal pathology and renal function biomarker level of the mice at different timepoints post intravenous injection of (+)-AuNPs and (-)-AuNPs.

Supplementary Fig.11. Accumulation of the AuNPs in major organs and tissue of the mice at different timepoints post intravenous injection at different timepoints post intravenous injection of (+)-AuNPs and (-)-AuNPs.

Supplementary Fig.12. Endocytosis of (+)-AuNPs by proximal tubules at 24h post intravenous injection.

Supplementary Fig.13. Biotransformation of (+)-AuNPs in the endosomes/lysosomes of proximal tubules at 24h post intravenous injection.

Supplementary Fig.14. Magnified EM images showing the assemblies of AuNPs into nanofibers to form the typical flower-like large nanoassemblies.

Supplementary Fig.15. Comparison of biotransformed (+)-AuNPs in endosomes and lysosomes at 24h post intravenous injection[1].

Supplementary Fig.16. Biotransformation of (-)-AuNPs in the endosomes/lysosomes of proximal tubules at 24h post intravenous injection.

Supplementary Fig.17. Biotransformation of (+)-AuNPs in Kupffer cells in the liver at 24h post intravenous injection.

Supplementary Fig.18. Biotransformation of (+)-AuNPs in the endosomes/lysosomes of proximal tubules of genetically metallothionein knock-out mice at 24h post intravenous injection.

Supplementary Fig.19. Incubation of AuNPs with glutathione, hydrogen peroxide and metallothionein.

Supplementary Fig.20. Extracellular vesicles in proximal tubular lumen at 24h post intravenous injection of (+)-AuNPs.

Supplementary Fig.21. Representative EM images of distal tubules at 24h post intravenous injection of (+)-AuNPs.

Supplementary Fig.22. Representative EM images of collecting ducts at 24h post intravenous injection of (+)-AuNPs.

Supplementary Fig.23. The AuNPs with different morphologies in the urine collected within 24h post intravenous injection of (+)-AuNPs.

Supplementary Fig.24. Organelle extrusion of proximal tubular epithelial cells of the mice at 24h post intravenous injection of (+)-AuNPs.

Supplementary Fig.25. Endocytosed (+)-AuNPs on the luminal side of proximal tubules were not reabsorbed back to blood circulation through tubular reabsorption.

Supplementary Fig.26. Cellular uptake and extrusion in different segments of proximal tubules at 24h post intravenous injection of (+)-AuNPs[2].

Supplementary Fig.27. Extracellular vesicles with organelles observed in vitro in human kidney proximal tubular cells (HK-2).

Supplementary Fig.28. Organelle extrusion of proximal tubular epithelial cells in PBS-injected mice.

Supplementary Fig.29. Organelle extrusion of proximal tubular epithelial cells in (-)-AuNPs-injected mice.

Supplementary Fig.30. Quantification of the percentage of extruded vesicles without mitochondria in PBS, (-)-AuNPs and (+)-AuNPs-injected mice.

Supplementary Fig.31. Extruded vesicles containing different types of organelles.

Supplementary Fig.32. Extrusion of a nucleus.

Supplementary Fig.33. Renal pathology and renal function biomarker level of the mice at 24h post intravenous injection of PBS, (-)-AuNPs and (+)-AuNPs.

Supplementary Fig.34. Establishment and characterizations of cisplatin-induced proximal tubular injury model.

Supplementary Fig.35. Extrusion and biotransformation in proximal tubules with appearing normal morphology in mouse model of cisplatin-induced acute tubular injury at 24h post intravenous injection of (+)-AuNPs.

Supplementary Fig.36. Extrusion and biotransformation in mildly damaged proximal tubules in mouse model of cisplatin-induced acute tubular injury at 24h post intravenous injection of (+)-AuNPs.

Supplementary Fig.37. Autophagosomes and apoptotic bodies in severely damaged proximal tubules in mouse model of cisplatin-induced acute tubular injury at 24h post intravenous injection of (+)-AuNPs.

Supplementary Fig.38. Quantification of the uptake efficiencies of (+)-AuNPs in normal, mildly damaged, and severely damaged proximal tubules in mouse model of cisplatin-induced acute tubular injury.

3. Supplementary References

1. Materials and Methods

1.1. Materials and equipment

Gold (III) chloride trihydrate (product number: 520918), poly (ethylene glycol) methyl ether thiol (average molecular weight: 800 Dalton, product number: 729108), 11-Amino-1-undecanethiol hydrochloride (product number: 674397), chlorpromazine hydrochloride (CPZ, product number: C8138), cis-Diamineplatinum(II) dichloride (cisplatin, product number: 479306), silver nitrate (product number: 209139), L-Glutathione reduced (GSH, product number: G4251), Amicon® Ultra-4 centrifugal filters (molecular weight cut-off: 10k Dalton, product number: UFC8010) and Amicon® Ultra-15 centrifugal filters (molecular weight cut-off: 100k Dalton, product number: UFC901024) were purchased from MilliporeSigma (USA). Fisherbrand™ Regenerated Cellulose Dialysis Tubing (molecular weight cut-off: 3500 Dalton, catalog number: 21-152-10), DTS1070 folded capillary cell (catalog number: NC0491866) and hydroquinone (catalog number: H329-500) were purchased from Thermal Fisher Scientific. Sephadex LH-20 (product number: 17009002) was purchased from cytiva. Hydrogen peroxide solution (catalog number: 31642-500 ml) was purchased from Honeywell. The anti-metallothionein antibody (ab192385) and the IHC polymer detection kit HRP/DAB (ab209101) were purchased from Abcam. Absorption spectra were collected by a Virian 50 Bio UV-vis spectrophotometer. Core size of AuNPs was measured using a JEOL 2100F field emission TEM/STEM. Hydrodynamic diameters and zeta-potential of AuNPs were measured by a Malvern ZS90 particle size analyzer. The ^{1}H NMR spectra were collected using a Bruker Avance III HD 600 MHz NMR instrument. Gold amount in tissue and organ samples was quantified using an Agilent 7900 inductively coupled plasma mass spectrometry (ICP-MS). Optical images of tissue slides were imaged using Olympus VS120 virtual slide scanner. Electron microscopic imaging of kidney tissue was conducted using a JEOL 1400 Plus instrument equipped with an AMT BIOSPRINT16M-ActiveVu mid mount CCD camera. Human kidney proximal tubular (HK-2) cells were originally purchased from ATCC (ATCC CRL-2190). Animal studies were performed according to the guidelines of the University of Texas System Institutional Animal Care and Use Committee (authorized protocol number: 11-08). Genetically metallothionein knock-out mice 129S7/SvEvBrd-Mt1<tm1Bri> Mt2<tm1Bri>/J (strain code 002211) of 6-8 weeks old, weighing 20-25g, were purchased from the Jackson Laboratory. BALB/c mice (BALB/cAnNCr, strain code 047) of 6-8 weeks old, weighing 20-25g, were purchased from Envigo. All mice were randomly allocated and housed under standard environmental conditions (23±1 °C, 50±5% humidity and a 12/12 h light/dark cycle) with free access to water and standard laboratory food. Original softwares of instruments used to collect all the data in this work include Varian UV Cary 50 version 3.00 for absorption spectra collection, Malvern Zetasizer version 7.04 for DLS measurement. Agilent MassHunter Workstation 4.2 for inductive coupled plasma mass spectroscopy measurements, VS-ASW-L100 of Olympus VS120-L100 Slide Scanner for histological imaging and AMT Capture Engine Version 7.00 of JEM-1400+ transmission electron microscope. OriginLab 2020, NanoMeasure 1.2, cellSense Dimension, and ImageJ 1.50 were used for data analysis. Adobe Illustrator CC 2017 was used for drawing figures.

1.2. Synthesis of pegylated negatively charged AuNPs [(-)-AuNPs]

Pegylated negatively charged AuNPs was synthesized according to our previous report[3, 4]. Briefly, 45 ml of distilled water was heated to 95 °C in oil bath. Poly (ethylene glycol) methyl ether thiol aqueous solution of 4.17 ml and 24 mM was then added to the water solution and stirred under 1600 rpm for 5 min. Gold (III) chloride trihydrate aqueous solution of 150 µl and 1 M was then added to the water solution and stirred under 1600 rpm. The reaction was allowed to proceed for 30 min. After 30 min, the reaction container was lifted from the oil bath and cooled to room temperature. For the purification, the reaction mixture was transferred from the reaction container to centrifuge tubes and centrifuged under 21000 g for 5min to remove large aggregates. After that, the supernatant was transferred to a Dialysis Tubing (molecular weight cut-off: 3500 Dalton) and dialyzed in water for 48 h (replace the water solution for at least 4 times during 48 h). After dialysis the (-)-AuNPs solution was purified using two centrifugal filters (molecular weight cut-off: 10 k and 100 k Dalton) with 1 x phosphate buffered saline buffer (PBS) as washing medium. The (-)-AuNPs that can pass through the 100 k Dalton filter but cannot pass through the 10 k Dalton filter were collected and then purified with sephadex LH-20 size-exclusive columns. The purified (-)-AuNPs solution was stored under -20°C for animal studies.

1.3. Synthesis of pegylated positively charged AuNPs [(+)-AuNPs]

The 50 µl 50 mM 11-Amino-1-undecanethiol hydrochloride in ethanol was added to 250 µl 2.5 mg / ml (-)-AuNPs (dissolved in ethanol as well). The reaction mixture was vortexed at the speed of 500 for overnight. For the purification, 9.7 ml PBS buffer was first added to the 300 µl reaction mixture. The PBS / ethanol mixture was centrifuged under 21000 g for 5 min to remove the water-insoluble unreacted 11-Amino-1-undecanethiol hydrochloride ligands as well as potential water-insoluble over-etched (+)-AuNPs. After that, the supernatant was purified using two centrifugal filters (molecular weight cut-off: 10 k and 100 k Dalton) with PBS buffer as washing medium. The AuNPs that can pass through the 100 k Dalton filter but cannot pass through the 10 k Dalton filter were collected and then purified with sephadex LH-20 size-exclusive columns. The purified (+)-AuNPs solution was stored under -20°C and used for animal studies.

1.4. Characterization of absorption spectra of the synthesized AuNPs

Absorption spectra of the synthesized AuNPs were collected by a Varian Cary 50 Bio UV-Vis spectrophotometer using a 1 mm cuvette. The scanning range was from 800 to 200 nm. The concentration of AuNPs was adjusted to make sure the maximum absorption of AuNPs at 200 nm is below 1.

1.5. Size characterization of the synthesized AuNPs

Core size of AuNPs was measured using a JEOL 2100F field emission TEM/STEM. AuNPs dissolved in water and deposited on the TEM grids. The distribution of core size of AuNPs was analyzed using NanoMeasurer 1.2 software. Hydrodynamic diameters (HD) of AuNPs were measured by a Malvern ZS90 particle size analyzer. AuNPs dissolved in 1x PBS buffer for HD measurement. The average core size or HD was the $xc \pm w/2$ obtained by fitting the histogram with a Gaussian distribution in Origin.

1.6. Characterization of the surface ligand ratio of (+)-AuNPs

(+)-AuNPs, (-)-AuNPs and poly (ethylene glycol) methyl ether thiol were dispersed in deuterium oxide. 11-Amino-1-undecanethiol was dispersed in deuterated chloroform. The ^{1}H-NMR spectra were obtained using a Bruker Avance III HD 600 MHz NMR instrument.

1.7. Zeta-potential measurement of the synthesized AuNPs

Zeta-potential of AuNPs were measured by using DTS1070 folded capillary cells and a Malvern ZS90 particle size analyzer. AuNPs were dispersed in 1X PBS buffer.

1.8. Renal clearance efficiency measurement of the synthesized AuNPs

Balb/c mice (6-8 weeks old, weighing 20-25g, n = 3) were intravenously injected with AuNPs (~0.5 mg/mL, 200 µl). Urine samples within 24 h post injection of AuNPs were collected using metabolic cages. The amount of AuNPs in the urine samples were determined by ICP-MS[5].

1.9. Biodistribution studies of the synthesized AuNPs in mice

To quantify the biodistribution of the AuNPs in mice, balb/c mice (6-8 weeks old, weighing 20-25g, $n \geq 3$) injected with AuNPs (~0.5 mg/mL, 200 µl) at different time points post injection were sacrificed and dissected. The blood, essential organs and tissue were collected and digested with aqua regia. The digested organs and tissue were further diluted with water and centrifuged to remove the undegradable substances. The supernatant was preserved and the amount of gold in the supernatant was measured by ICP-MS[5].

1.10. Histological tissue studies of the kidney

Balb/c mice (6-8 weeks old, weighing 20-25g) injected with the synthesized AuNPs (~0.5mg/ml, 200 µl) were sacrificed at different time points post injection. The kidneys were harvested and fixed in 10% formalin for at least 24h. The fixed kidneys were then processed in tissue processor for dehydration and paraffin embedding. The fixed kidneys were then sectioned into 4 µm sections that contained entire cross sections of the kidneys including different compartments of the kidneys (cortex, outer medulla, inner medulla, papilla, and pelvis). The kidney tissue sections were first stained by silver nitrate and hydroquinone (silver enhancement) for clear visualization of the ultrasmall AuNPs under slide scanner microscopic imaging to obtain images of the entire cross sections of the kidneys. Specifically, kidney tissue sections were first dewaxed in xylene for 8min to remove the surrounding wax. The silver nitrate solution of 50 µL and 0.1 M and hydroquinone solution of 50 µL and 0.2 g/L was mixed and added on the kidney tissue sections to stain the tissue for 2-15 min to obtain an optimal contrast of the AuNPs. To compare the accumulations of the synthesized AuNPs in the proximal tubules and other nephron components, we used the same period of silver enhancement staining for the kidney tissue sections that need to be compared. After that, the kidney tissue sections were rinsed with ultrapure water to remove the silver staining solution. Kidney tissue sections after silver staining were subsequently stained with hematoxylin and eosin (H&E) to visualize the physiological structures. The H&E-stained kidney tissue sections were sealed by cover glass and imaged with Olympus VS120 virtual slide scanner microscope.

1.11. Quantification of area fraction of the synthesized AuNPs in proximal tubules

Quantification of area fraction of the synthesized AuNPs in proximal tubules was conducted using Olympus Cellsens software. An entire area of a cross section of proximal tubule was first selected to give the region of interest (ROI). Then, the silver enhanced AuNPs in the ROI were selected and highlighted. Finally, the area fraction of the highlighted silver enhanced AuNPs to the ROI area (entire area of the cross section of proximal tubule) was calculated using the software.

1.12. Establishment of chlorpromazine (CPZ)-treated mouse model

Balb/c mice (6-8 weeks old, weighing 20-25 g, $n \geq 3$) were intraperitoneally injected with 20 mg / kg chlorpromazine. At 30 min post injection of chlorpromazine, mice were intravenously injected with (+)-AuNPs (~0.5 mg/ml, 200 µl) and were under anaesthesia by inhalation of isoflurane for 2 h. At 2 h post injection of (+)-AuNPs, mice were dissected, the urine, blood and essential organs were harvested. Amounts of AuNPs in the urine, blood and organs were determined by ICP-MS.

1.13. Electron microscopic (EM) imaging of the kidney and liver tissue of normal mice and the kidney tissue of metallothionein knock-out mice after intravenous injection of the synthesized AuNPs or phosphate-buffered saline (PBS)

Balb/c mice (6-8 weeks old, weighing 20-25g) and genetically metallothionein knock-out mice 129S7/SvEvBrd-Mt1<tm1Bri> Mt2<tm1Bri>/J (6-8 weeks old, weighing 20-25g) were injected with the synthesized AuNPs (~0.5mg/ml, 200 µl) or PBS and then were sacrificed and fixed via transcardial perfusion at 24h post injection. Specifically, 10 mL heparizinzed normal saline was first used to perfuse the mice under a perfusion speed of 75 mL/h using a syringe pump, followed by the perfusion of 10 mL 4% paraformaldehyde/PBS fixative at the same perfusion speed. After the perfusion process, the kidneys and liver of normal mice and the kidneys of metallothionein knock-out mice were harvested and cut into $1mm^3$ cubes (cortex area of the kidney was selected for EM imaging of proximal tubules). The tissue cubes were immersed in 4% paraformaldehyde/PBS and keep at 4 °C for at least 24h for further fixation. The tissue cubes were subsequently washed with sodium cacodylate buffer and stained with osmium tetroxide and potassium ferricyanide in sodium cacodylate buffer for 1.5h at room temperature, followed by being rinsed with water and en bloc stained with 4% uranyl acetate in 50% ethanol for 2h. The tissues were then dehydrated with increasing concentrations of ethanol, transitioned into resin with propylene oxide, infiltrated with Embed-812 resin and polymerized in a 60 °C oven overnight. Lastly, the blocks were sectioned with a diamond knife (Diatome) on a Leica Ultracut 6 ultramicrotome (Leica Microsystems) and collected onto grids. No membrane staining with uranyl acetate and lead citrate and gold or silver enhancement for AuNPs were used. EM images were taken using a JEOL

1400 Plus instrument equipped with an AMT BIOSPRINT16M-ActiveVu mid mount CCD camera and electron dispersion X-ray spectroscopic spectrums were obtained using a 200kV Jeol 2100 transmission electron microscope[3].

1.14. Incubation of AuNPs with glutathione, hydrogen peroxide and metallothionein

(+)-AuNPs and (-)-AuNPs (100 µl, ~2.5 mg/ml in 1x PBS) were incubated with 1x PBS (100 µl), glutathione (100 µl, 10 mM in 1x PBS), hydrogen peroxide (100 µl, 30% w/w) and metallothionein (100 µl, 70 µM in 1x PBS), respectively. The pH of the incubation mixture was adjusted to 4.5 to mimic the lysosome pH. The mixture was allowed to incubate for 24h at room temperature. After 24 h of incubation, the mixture solution was deposited on TEM grids for EM imaging. The absorption spectra of the mixture solutions were collected to compare the difference in the absorption of (+)-AuNPs before and after incubation.

1.15. Immunohistochemical staining of metallothionein in kidney tissue section

Immunohistochemical staining of paraffin-embedded kidney sections with anti-metallothionein antibody was performed according to the following protocol: Deparaffinize slides in 2 changes of xylene, 5 min each. Transfer slides to 100% alcohol, for 2 changes, 3 min each, and then transfer once through 95%, 70%, and 50% alcohols respectively for 3 min each. Wash sections twice in DI water for 5 minutes each. Block endogenous peroxidase activity by incubating sections in 3% hydrogen peroxide solution in methanol at room temperature for 30 min to block endogenous peroxidase activity. Wash sections twice in DI water for 5 minutes each. Rinse in 300 ml of PBS for 3 changes, 5 min each. Add 100 µl blocking buffer (5% fetal bovine serum in PBS) onto the sections of the slides and incubate in a humidified chamber at room temperature for 30 minutes. Drain off the blocking buffer from the slides. Apply 100 µl 100x diluted primary antibody in antibody dilution buffer (0.5% bovine serum albumin in PBS) to the sections on the slides and incubate in a humidified chamber at 4 ℃ overnight in refrigerator. Wash 3 times in PBS. Apply Amplifier from ab209101 kit and incubate for 10 minutes at room temperature. Wash 3 times with PBS. Apply Detector from ab209101 kit and incubate for 10 minutes at room temperature. Wash 3 times in PBS. Apply chromogen (DAB) to the tissue and incubate for 5-10 minutes, depending on the desired stain intensity. Wash slides in 300 ml PBS 3 times for 2 minutes each time. Counterstain slides by immersing slides in Hematoxylin for 1-2 minutes. Rinse the slides in running tap water for more than 15 minutes. Dehydrate the tissue slides through 4 changes of alcohol (95%, 95%, 100% and 100%), 5 minutes in each one. Clear the tissue slides in 3 changes of xylene and mount coverslip using mounting media. Observe the color of the antibody staining under microscopy.

1.16. In vitro cellular EM study of (+)-AuNPs in monolayer human kidney proximal tubular cells (HK-2) after in situ fixation and embedding

(+)-AuNPs (100 µl, ~1 mg/ml in PBS) were added to HK-2 cells grown on 2 ml petri dishes. After overnight incubation, the cell medium was removed. The cells were washed with 2 ml PBS for three times and fixed with PFA solution for 30 mins under room temperature. Cells were fixed on MatTek dishes with 2.5% (v/v) glutaraldehyde in 0.1M sodium cacodylate buffer. After five rinses in 0.1 M sodium cacodylate buffer, they were post-fixed in 1% osmium tetroxide plus 0.8 % K3[Fe(CN6)] in 0.1 M sodium cacodylate buffer for 1 h at room temperature. Cells were rinsed with water and en bloc stained with 2% aqueous uranyl acetate for 1 h. After five rinses with water, specimens were dehydrated with increasing concentration of ethanol, infiltrated with Embed-812 resin, and polymerized in a 60 ℃ oven overnight. Epoxy discs were removed by submerging MatTek dishes in liquid nitrogen. Pieces of the disc were super glued to a blank block. Blocks were sectioned with a diamond knife (Diatome) on a Leica Ultracut UCT (7) ultramicrotome (Leica Microsystems) and collected onto copper grids, post stained with 2% Uranyl acetate in water and lead citrate. Images were acquired on a JEOL 1400+ transmission electron microscope equipped with a LaB6 source using a voltage of 120 kV and an AMT-BioSprint 16M CCD camera. The fixed monolayer cells remained in place throughout processing and embedding. No membrane staining with uranyl acetate and lead citrate and gold or silver enhancement for AuNPs were used.

1.17. Establishment and characterization of cisplatin-induced acute kidney injury model

The balb/c mice (6-8 weeks old, weighing 20-25g) were randomly divided into two groups (n ⩾ 3 for each group) and received intraperitoneal injection of PBS or 20 mg/kg of cisplatin. The body weight of mice was measured, and blood samples were collected before injection of cisplatin and post 4 days injection of cisplatin for body weight monitoring and serum blood urea nitrogen measurement. At 4 days post injection of cisplatin or PBS, the mice were intravenously injected with (+)-AuNPs (~0.5mg/ml, 200 μl). At 24 h post injection of (+)-AuNPs, the kidneys of the mice were collected and processed for electron microscopy imaging and histological analysis.

1.18. Quantification of the area fraction of silver enhanced AuNPs in proximal tubules of normal mice

The quantification is conducted using Cellsens software. The entire area of cross section of a proximal tubule was first selected to give the region of interest (ROI). Then, the silver enhanced AuNPs in the ROI were automatically recognized by the software and highlighted in red. Finally, the area fraction of the highlighted silver enhanced AuNPs to the ROI area (entire area of cross section of the selected proximal tubule) was calculated using the software.

1.19. Statistical analysis

Error bars are reported as mean ± s.d. (standard deviation). The differences between groups were compared by analysis of two-sided Student's t-test and differences among three groups were compared by One-way ANOVA. ns (no significant), *P<0.05, **P<0.01, ***P<0.001, ****P<0.0001. Investigators conducting the experiments were not blinded. Dixon's Q test is used for identification and rejection of outliers in data analysis.

2. Supplementary Figures

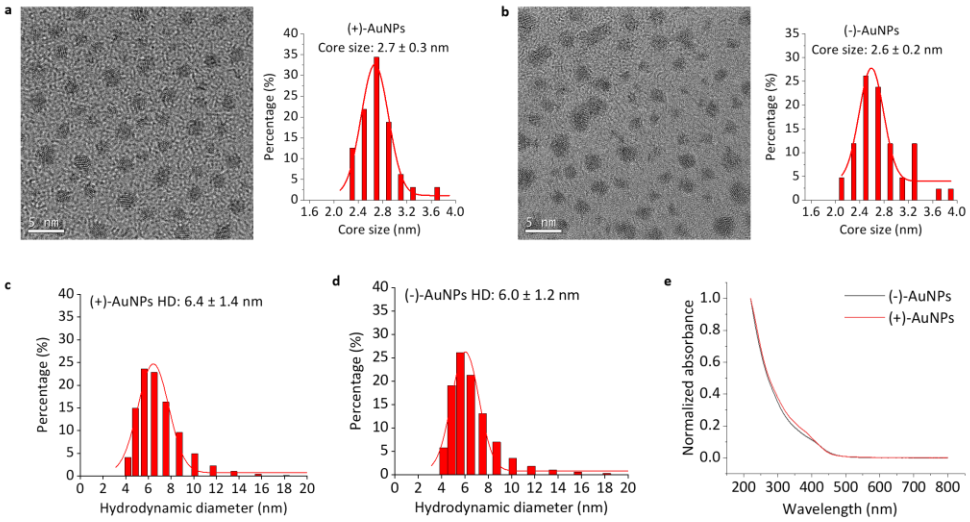

Supplementary Figure 1. Characterization of (+)-AuNPs and (-)-AuNPs. a, A representative TEM image and the size distribution of (+)-AuNPs. The core size of (+)-AuNPs is 2.7 ± 0.3 nm. **b**, A representative TEM image and the size distribution of (-)-AuNPs. The core size of (-)-AuNPs is 2.6 ± 0.2 nm, comparable to that of (+)-AuNPs. TEM imaging experiments are repeated for at least 2 times with similar results. **c**, The hydrodynamic diameter (HD) of (+)-AuNPs. The HD of (+)-AuNPs is 6.4 ± 1.4 nm, which is below the kidney filtration threshold (6 – 8 nm). **d**, The HD of (-)-AuNPs is 6.0 ± 1.2 nm, comparable to that of (+)-AuNPs. **e**, The absorption spectra of (+)-AuNPs and (-)-AuNPs. No surface plasma peak at ~529 nm is observed for both AuNPs, indicating the ultrasmall sizes of the AuNPs. In a-d, the average core size or HD was the xc ± w/2 obtained by fitting the histogram with a Gaussian distribution in Origin.

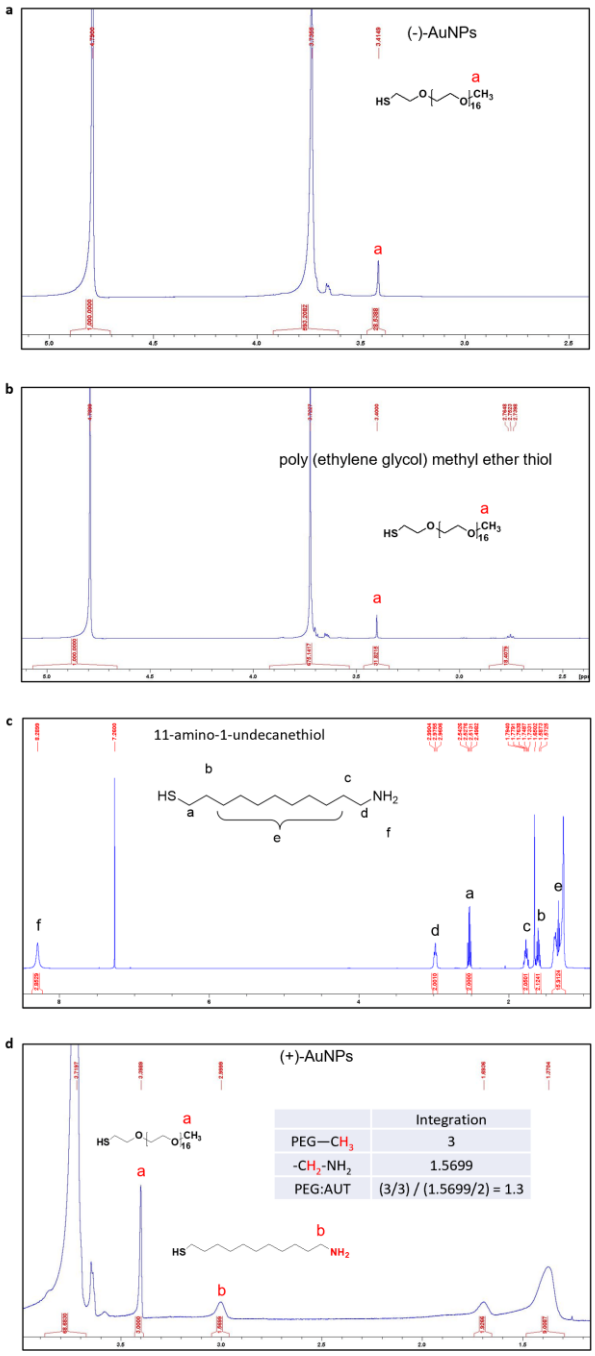

Supplementary Figure 2. Quantifying the PEG to 11-amino-1- undecanethiol ratio on (+)-AuNPs by ^{1}H-NMR in D2O. a, The ^{1}H-NMR spectrum of (-)-AuNPs in deuterium oxide. **b**, The ^{1}H-NMR spectrum of poly (ethylene glycol) methyl ether thiol ligand in deuterium oxide. The ^{1}H-NMR spectrum of (-)-AuNPs is identical to the spectrum of poly (ethylene glycol) methyl ether thiol because the (-)-AuNPs are coated with only poly (ethylene glycol) methyl ether thiol. **c**, The ^{1}H-NMR spectrum of 11-amino-1- undecanethiol in deuterated chloroform. **d**, The ^{1}H-NMR spectrum of (+)-AuNPs in deuterium oxide showing both ^{1}H-NMR peaks from poly (ethylene glycol) methyl ether thiol and 11-amino-1- undecanethiol. The ^{1}H-NMR signal of the terminal CH_3 group of PEG (position a) and the CH_2 group next to the terminal amine group (position b) of 11-amino-1-undecanethiol were identified as characteristic signals for the two surface ligands, respectively. The ratio between PEG : 11-amino-1-undecanethiol on the surface of (+)-AuNPs was calculated based on the integration and was determined to be 1.3 : 1 (PEG : 11-amino-1-undecanethiol (AUT)).

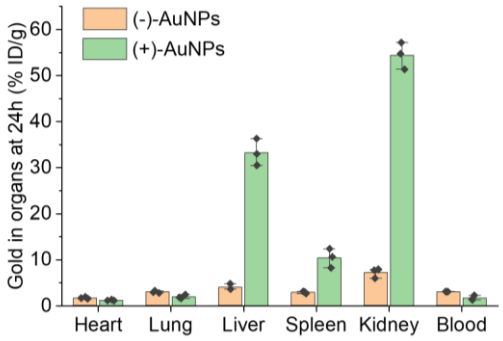

Supplementary Figure 3. Accumulation of (+)-AuNPs and (-)-AuNPs in blood, major organs and tissue of normal mice at 24h post intravenous injection. In addition to the high accumulation in the kidneys, (+)-AuNPs also showed higher accumulation in the liver and spleen than that of (-)-AuNPs. The distribution of (+)-AuNPs in the liver is 33.22 ± 2.38 %ID/g, which is ~8.5 times higher than that of (-)-AuNPs (3.91 ± 0.55 %ID/g) in the liver. The distribution of (+)-AuNPs in the spleen is 10.36 ± 1.69 %ID/g, which is ~3.7 times higher than that of (-)-AuNPs (2.83 ± 0.20 %ID/g) in the spleen. The distribution of (+)-AuNPs and (-)-AuNPs in the heart, lungs and blood is less than 3% ID/g. N=3 mice for each type of AuNPs, mean ± s.d. (standard deviation).

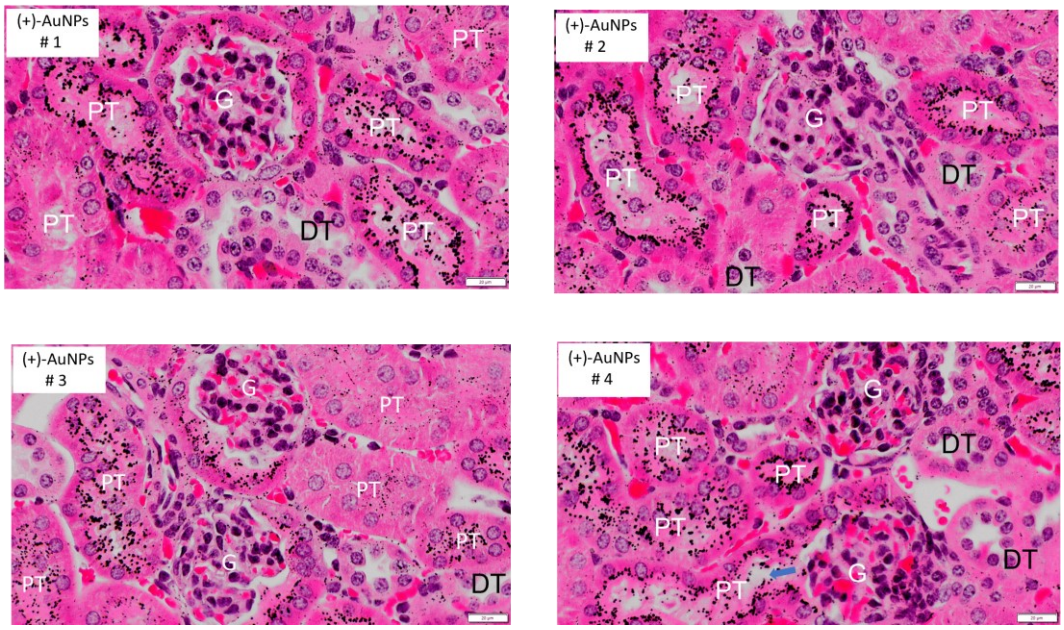

Supplementary Figure 4. Representative images of H&E-stained silver enhanced kidney tissue sections of normal mice showing distribution of (+)-AuNPs in the renal cortex at 24h post intravenous injection. The (+)-AuNPs (black dots, visualized by silver enhancement) mainly accumulated in the proximal tubules (PT). Very few silver-enhanced (+)-AuNPs are found in the distal tubules (DT) and the glomerulus (G), suggesting that proximal tubules are the major sites dedicating the accumulation of (+)-AuNPs in the kidneys. As shown in # 4 image, the blue arrow points the part of S1 segment of proximal tubule that is directly connect to the renal corpuscle. Representative images are presented out of images acquired from 3 independent samples.

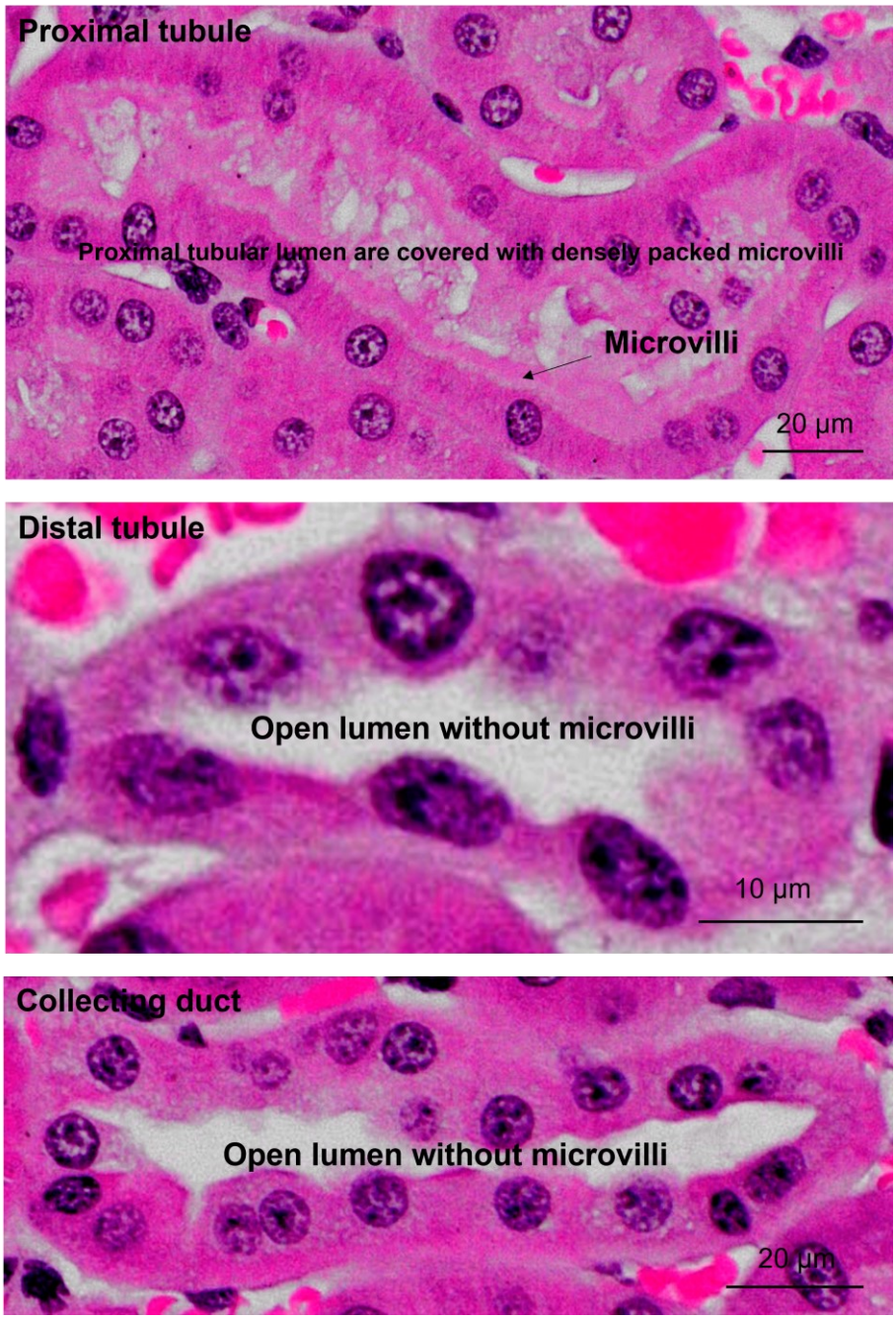

Supplementary figure 5. Representative high-resolution images of H&E-stained kidney tissue sections of normal mice showing histological difference among proximal tubules, distal tubules and collecting ducts. The most consistent and robust difference between the proximal tubules and distal tubules and collecting ducts is the presence of abundant microvilli on the luminal side of the proximal tubular epithelial cells. Representative images are presented out of images acquired from 3 independent samples.

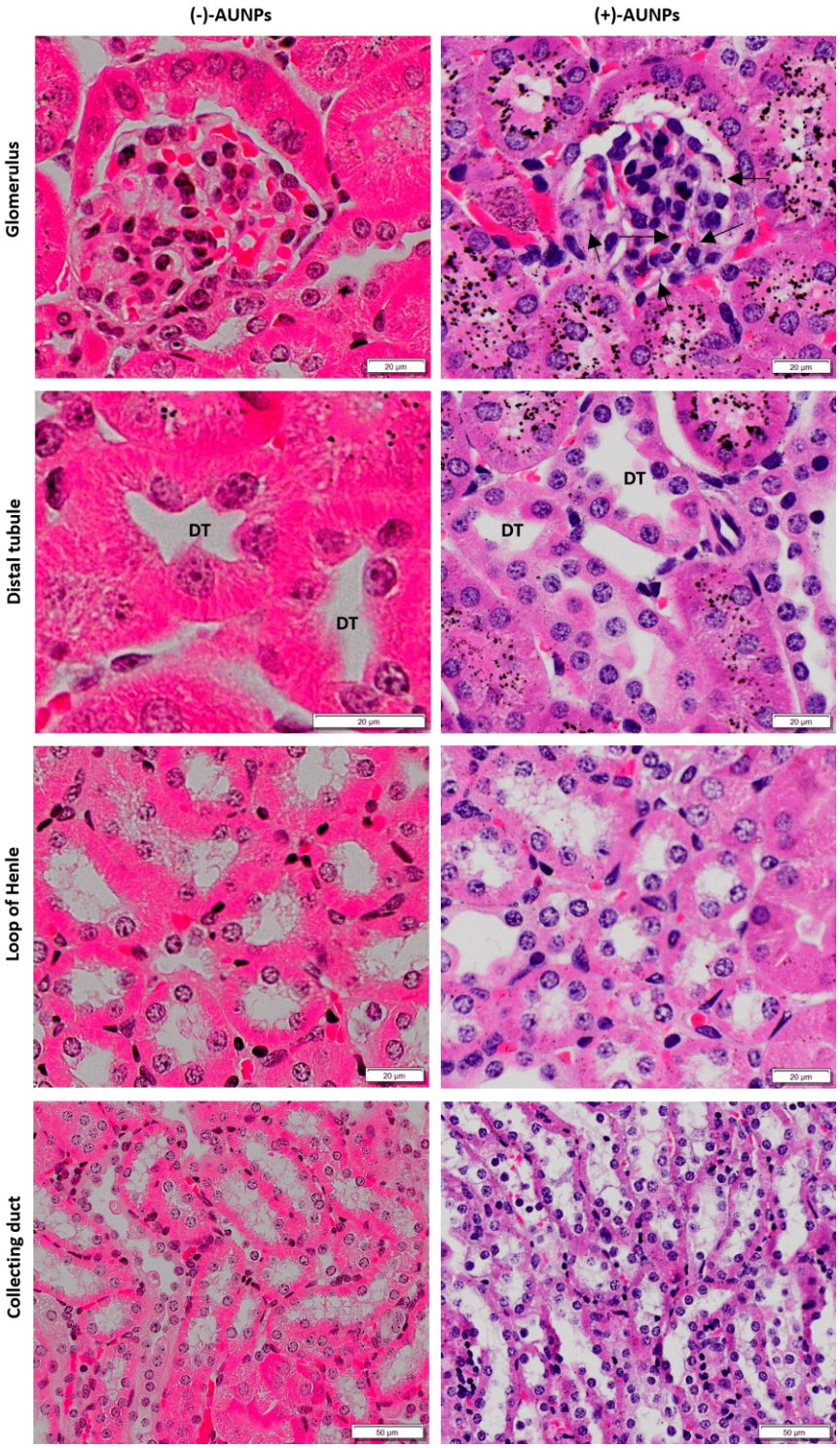

Supplementary Figure 6. Representative images of H&E-stained silver enhanced other renal compartments of normal mice including the glomerulus, the distal tubules (DT), the Loop of Henle and the collecting ducts at 24 h post intravenous injection of (-)-AuNPs and (+)-AuNPs. Low accumulation of (+)-AuNPs in the glomerulus was observed, which is dramatically lower compared to the proximal tubules around it. The rest compartments are not involved in the accumulation of AuNPs at normal status. Representative images are presented out of images acquired from 3 independent samples.

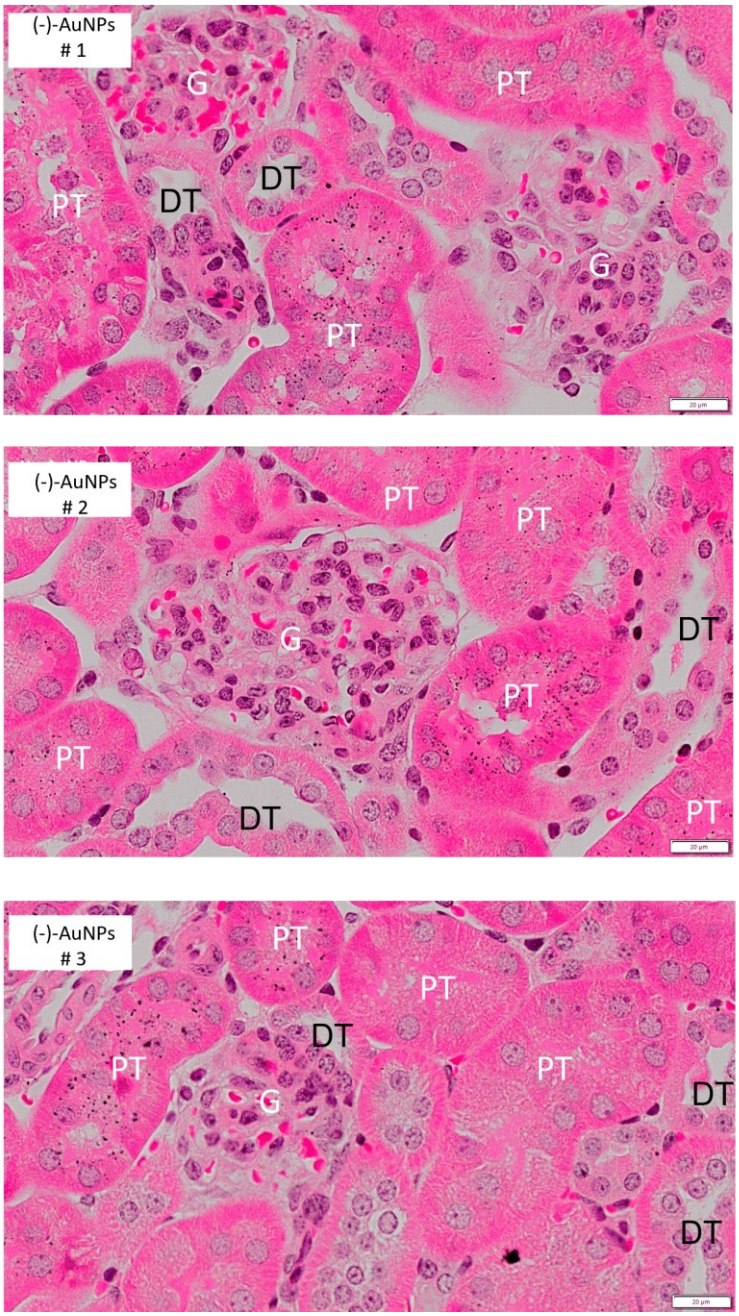

Supplementary Figure 7. Representative images of H&E-stained silver enhanced kidney tissue sections of normal mice showing distribution of (-)-AuNPs in the kidneys at 24h post intravenous injection. Similar to (+)-AuNPs, (-)-AuNPs (black dots, visualized by silver enhancement) also mainly accumulated in the proximal tubules (PT) and very few (-)-AuNPs were in the distal tubules (DT) and the glomerulus (G), further suggesting that proximal tubules are the major sites dedicating the accumulation of AuNPs in the kidneys. However, the accumulation of (-)-AuNPs in the proximal tubules is much lower compared to (+)-AuNPs with the same injection dose. Taken together, proximal tubules are the major sites dedicating the accumulation of renal-clearable AuNPs in the kidneys and positive surface charge of the AuNPs facilitates their accumulation in the proximal tubules. Representative images are presented out of images acquired from 3 independent samples.

Step 1: Select proximal tubules of interest.

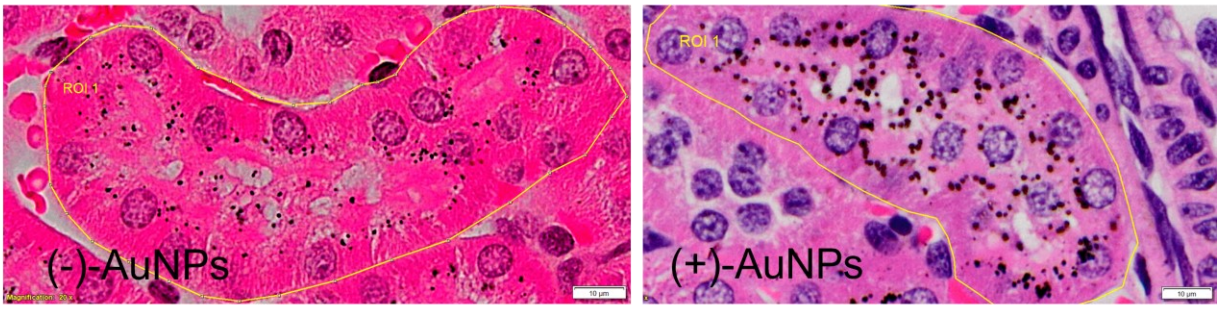

Step 2: Highlight the silver enhanced AuNPs.

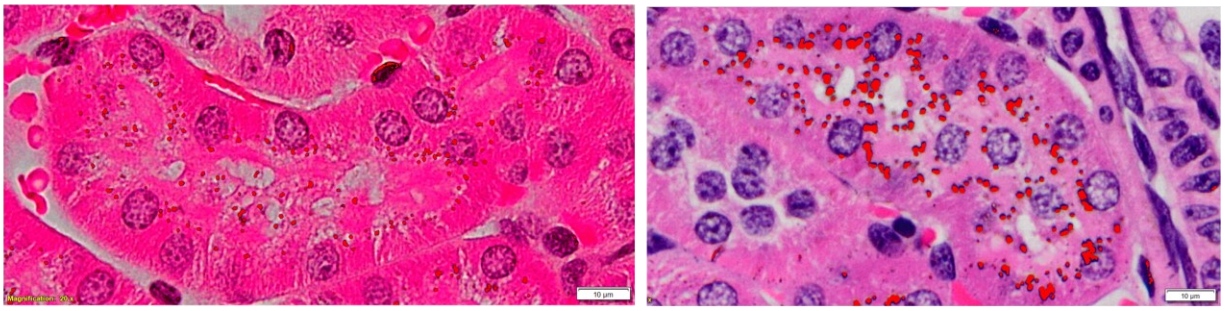

Step 3: Calculate the area fraction between the area of silver enhanced AuNPs to the area of the selected proximal tubule of interest using Cellsens software.

Count and Measure Results

Object Measurements | Object Filter | Class Measurements | Class Histogram | ROI Measurements | ROI Histogram

	ROI	Sum (Area) [µm²]	Object Area Fraction ROI [%]	Mean (Mean (Gray Intensity Value))	Mean (Mean (Color Intensity Value))	Mean (Shape Factor)
1	ROI 1	109.01	1.04	-	158.35	0.59

Count and Measure Results

Object Measurements | Object Filter | Class Measurements | Class Histogram | ROI Measurements | ROI Histogram

	ROI	Sum (Area) [µm²]	Object Area Fraction ROI [%]	Mean (Mean (Gray Intensity Value))	Mean (Mean (Color Intensity Value))	Mean (Shape Factor)
1	ROI 1	180.09	4.52	-	136.59	0.67

Supplementary Figure 8. Quantification of the area fraction of silver enhanced AuNPs in proximal tubules of normal mice. The quantification is conducted using Cellsens software. The entire area of cross section of a proximal tubule was first selected to give the region of interest (ROI). Then, the silver enhanced AuNPs in the ROI were automatically recognized by the software and highlighted in red. Finally, the area fraction of the highlighted silver enhanced AuNPs to the ROI area (entire area of cross section of the selected proximal tubule) was calculated using the software.

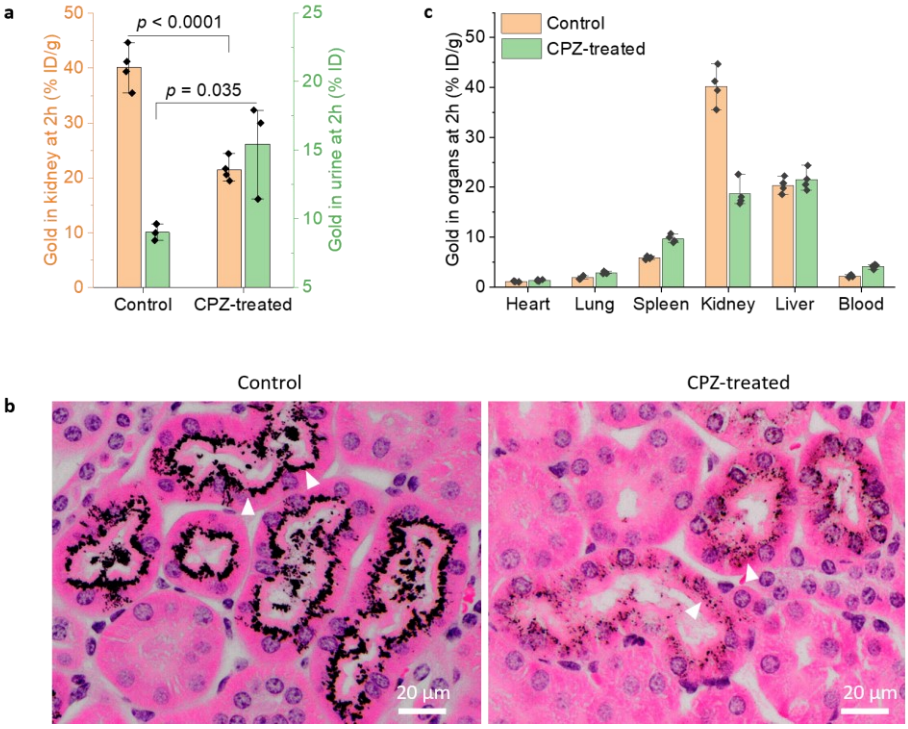

Supplementary Figure 9. Effect of inhibiting clathrin-mediated endocytosis using chlorpromazine (CPZ) on the kidney accumulation, renal clearance efficiency and distribution in proximal tubules of (+)-AuNPs. **a**, Once the mice were treated with CPZ (20 mg / kg, intraperitoneal injection at 30 min before injection of (+)-AuNPs), the kidney accumulation of (+)-AuNPs decreased from 40.37 ± 3.31 %ID/g to 21.52 ± 1.84 %ID/g (p = 4.96E-4) while the renal clearance efficiency of (+)-AuNPs was increased from 9.0 ± 0.5 %ID to 15.4 ± 2.9 %ID at 2h post intravenous injection. N = 3 or 4 mice for each group, mean ± s.d. Two-sided Student`s t-test was performed at the 0.05 level. **b**, Representative images of H&E-stained and silver enhanced kidney tissue slides showing significantly reduced retention of (+)-AuNPs (black dots, visualized by silver enhancement, pointed by white triangles) in proximal tubules of CPZ-treated mice, implying that clathrin-mediated endocytosis was involved in the uptake of (+)-AuNPs by proximal tubules. c, The distribution of (+)-AuNPs in major organs and tissue in control and CPZ-treated group. The decrease in the distribution of (+)-AuNPs in the kidneys was most obvious compared to those in other organs. N = 3 or 4 mice for both control mice and CPZ-treated mice, mean ± s.d.

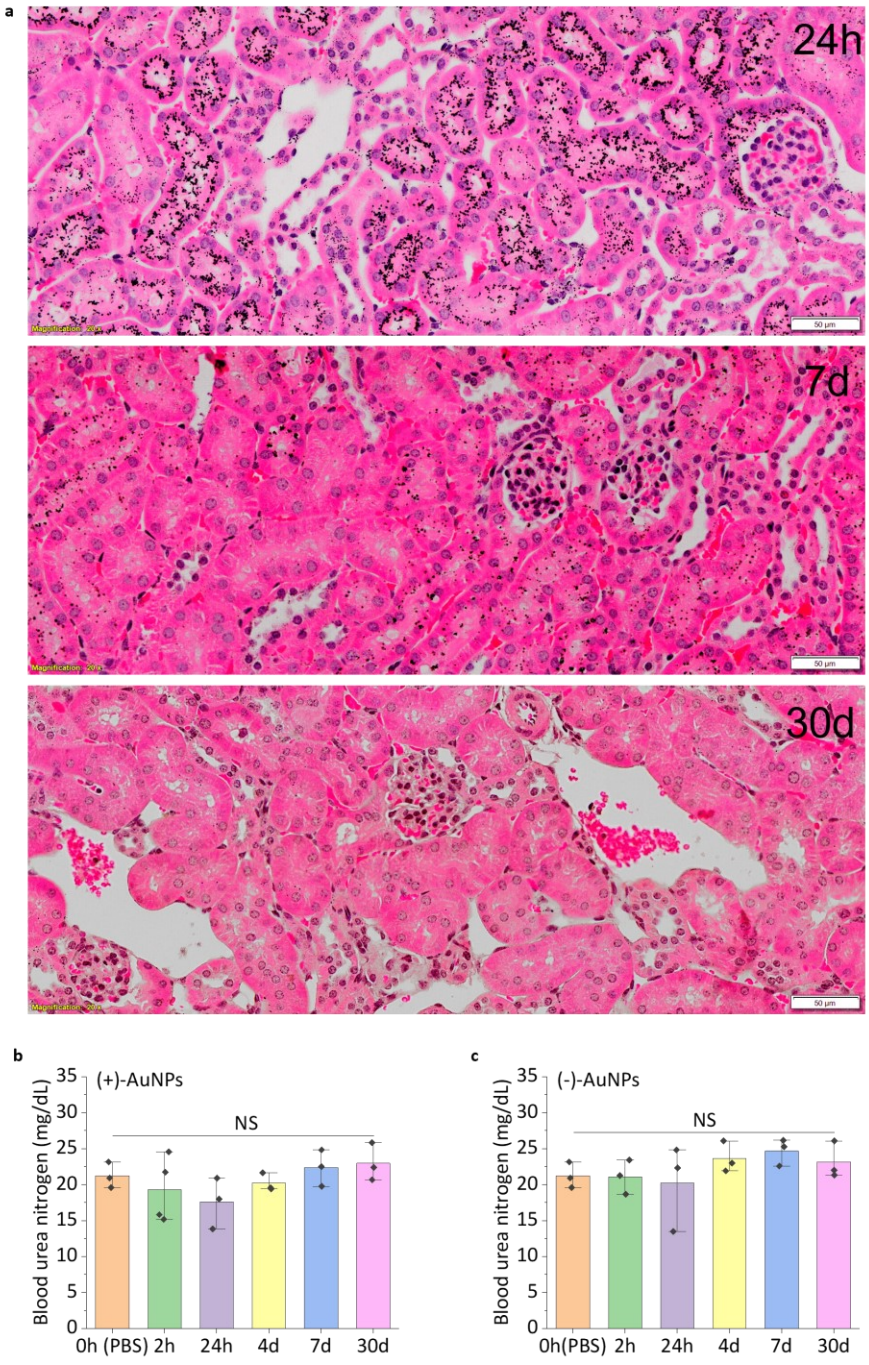

Supplementary Figure 10. Renal pathology and renal function biomarker level of the mice at different timepoints post intravenous injection of (+)-AuNPs and (-)-AuNPs. **a**, Representative images of H&E-stained and silver enhanced kidney tissue sections at 24h, 7d and 30d post injection of (+)-AuNPs (~0.5mg/ml, 200 μl for each mouse). No pathological damage in the kidney tissue was observed. The accumulation of (+)-AuNPs in proximal tubules (black dots, visualized by silver enhancement) were gradually and almost completely eliminated. **b and c**, The renal function biomaker blood urea nitrogen (BUN) levels in the serum of mice at different timepoints after injection of (+)-AuNPs (b, $p = 0.33$) and (-)-AuNPs (c, $p = 0.50$). 0h means the PBS control. The BUN level remained normal after injection of AuNPs. The pathology analysis and monitoring with BUN together proved that AuNPs caused no damage to the kidneys. N=3-4 mice for each time points, mean ± s.d. Data are analyzed using one-way ANOVA at the 0.05 significance level. NS, no significant difference.

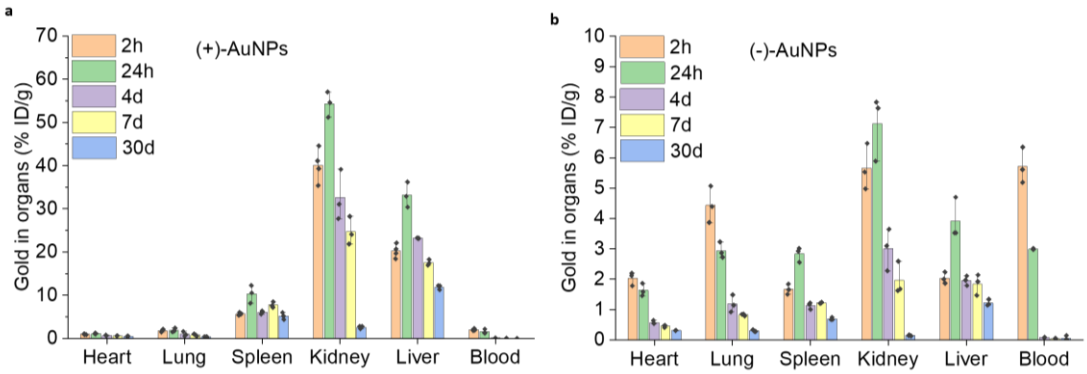

Supplementary Figure 11. Accumulation of the synthesized AuNPs in major organs and tissue of the mice at different timepoints post intravenous injection of (+)-AuNPs (a) and (-)-AuNPs (b). Both AuNPs were efficiently cleared out from the kidneys within one month post injection. N=3 mice for each type of AuNPs at different time points post injection, mean ± s.d..

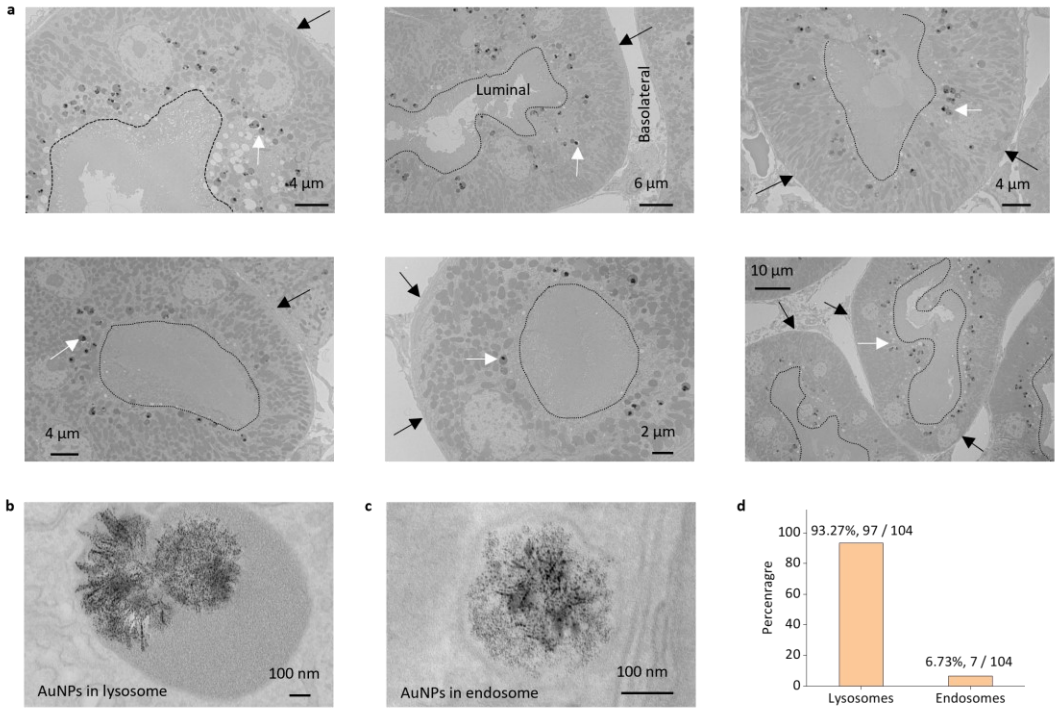

Supplementary Figure 12. Endocytosis of (+)-AuNPs by proximal tubules at 24h post intravenous injection. a, Representative EM images showing the endocytosis of (+)-AuNPs in intracellular vesicles (pointed by white arrows) on the luminal side of PTECs. The luminal side is labelled by dash line. The basolateral side is indicated by black arrows. The distribution of (+)-AuNPs on the luminal side of proximal tubules implies that (+)-AuNPs were endocytosed into PTECs from the luminal side after being filtered by the glomerulus rather than being taken into PTECs from the basolateral side. **b**, A representative EM image showing (+)-AuNPs in a lysosome. **c**, A representative EM image showing (+)-AuNPs in an endosome. Lysosomes have bigger size than endosomes and are typically electron-denser than endosomes due to high protein concentrations. **d**, Quantification of the percentage of AuNPs in lysosomes and endosomes. We analyzed 104 intracellular endocytic vesicles that contained the AuNPs and found 97 vesicles were lysosomes (93.27%) and 7 vesicles were endosomes (6.73%), indicating the majority of (+)-AuNPs were found in lysosomes at 24h post intravenous injection. Representative images in **a** are presented out of images acquired from 3 independent samples.

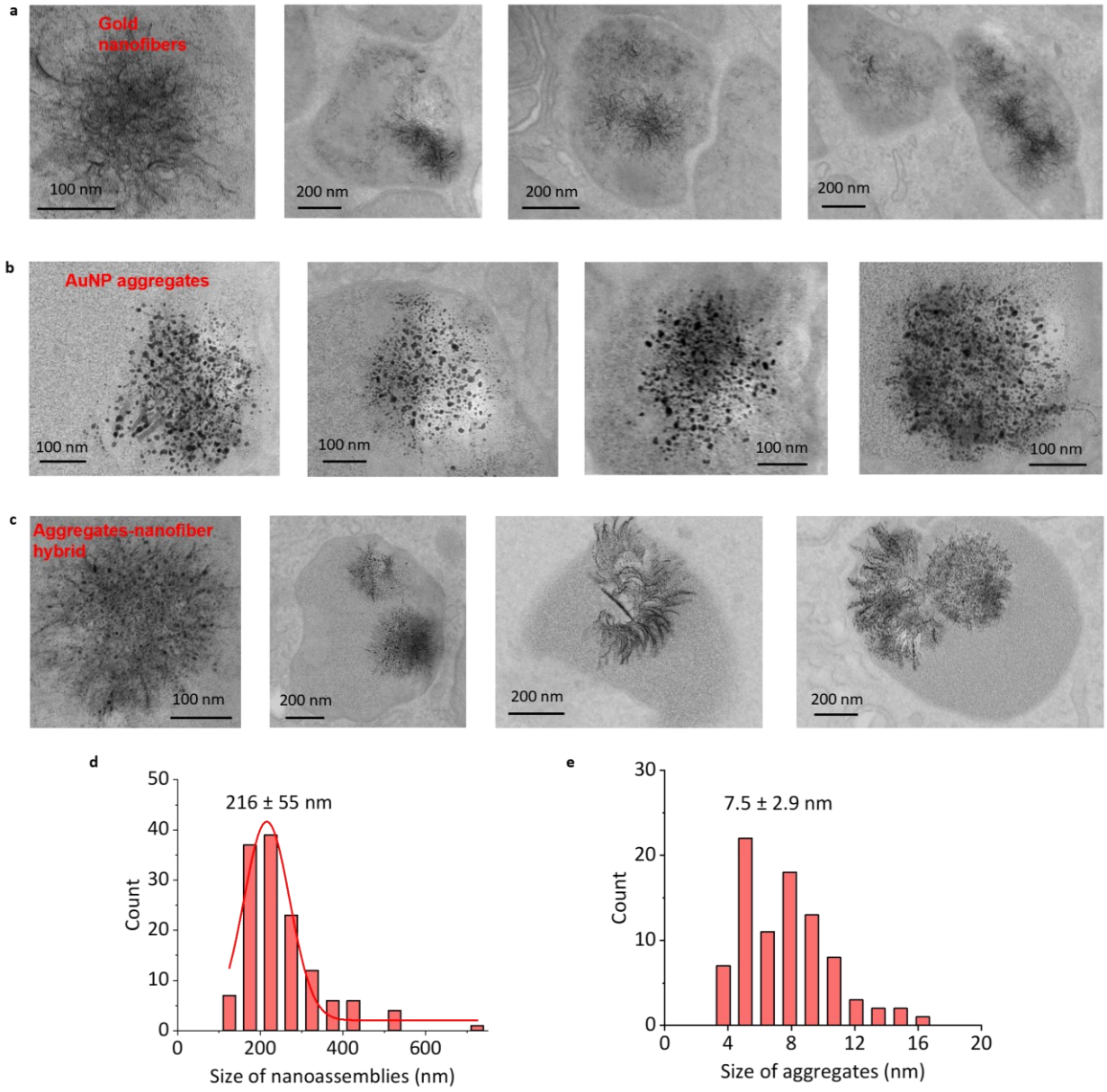

Supplementary Figure 13. Biotransformation of (+)-AuNPs in the endosomes/lysosomes of proximal tubules at 24h post intravenous injection. a, Representative EM images showing biotransformation of (+)-AuNPs into flower-like assemblies of gold nanofibers. **b**, Representative EM images showing nanoassemblies of 5-10 nm AuNPs formed by aggregation of 2-3 nm (+)-AuNPs ("AuNP aggregates") in lysosomes. **c**, Representative EM image showing hybrid assemblies of both nanofibers and AuNP aggregates. **d**, Quantification of the size of biotransformed nanoassemblies, the average size is 216 ± 55 nm. **e**, Quantification of the size of AuNP aggregates. The average size of the AuNP aggregates is 7.5 ± 2.9 nm. Representative images are presented out of images acquired from 3 independent samples.

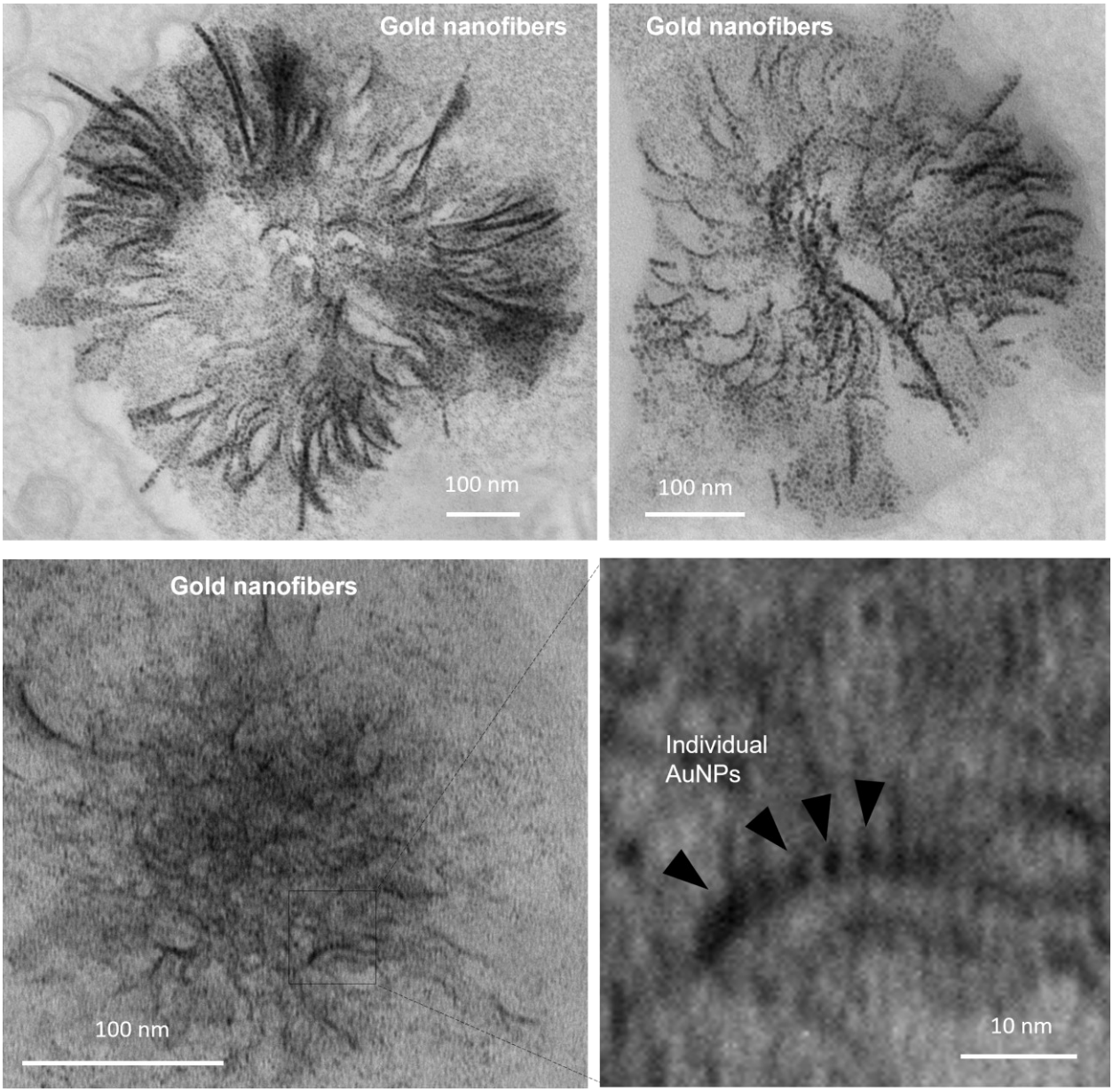

Supplementary Figure 14. Magnified EM images showing the assemblies of AuNPs into nanofibers to form the typical flower-like large nanoassemblies. Representative images are presented out of images acquired from 3 independent samples.

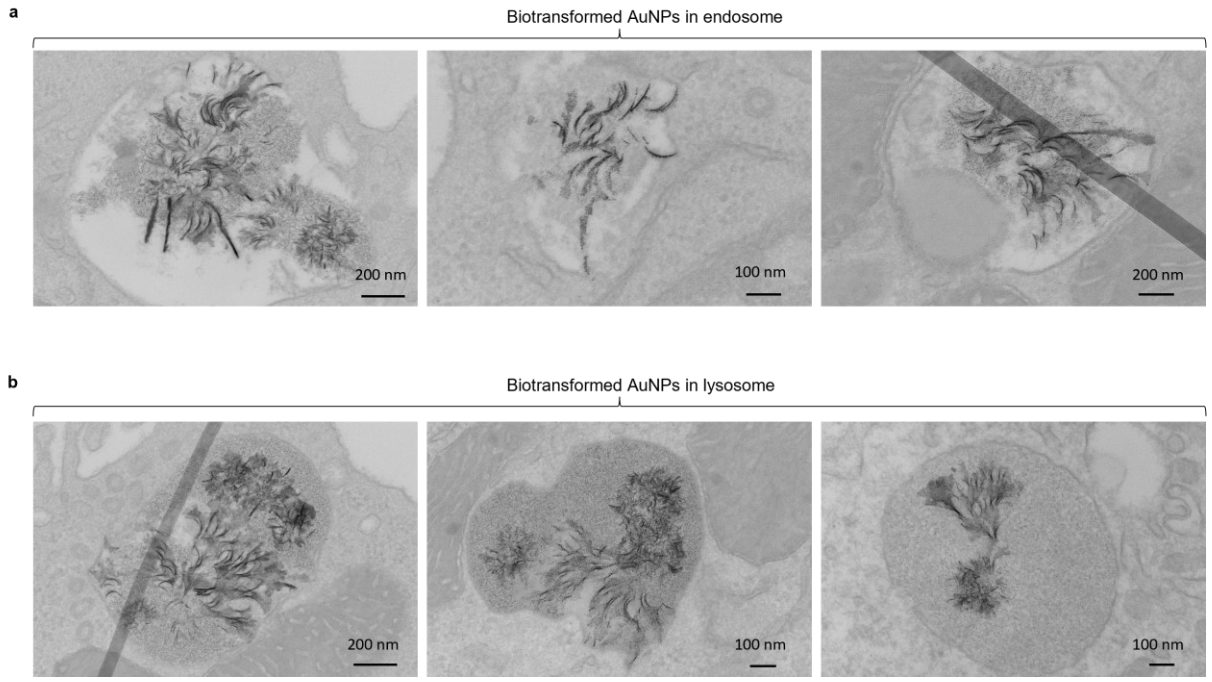

Supplementary Figure 15. Comparison of biotransformed AuNPs in endosomes and lysosomes. Lysosomes have bigger size than endosomes and are typically electron-denser than endosomes due to high protein concentrations under electron microscopy (Ref. 1). **a**, Biotransformed AuNPs in endosomes. **b**, Biotransformed AuNPs in lysosomes. No significant difference is observed between the morphology of biotransformed AuNPs in endosomes and lysosomes. Representative images are presented out of images acquired from 3 independent samples.

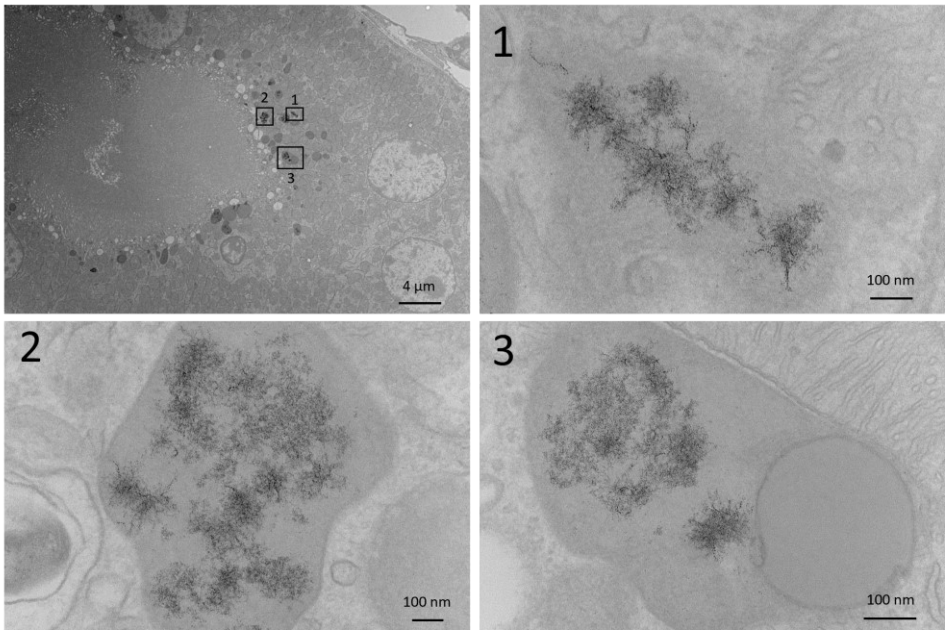

Supplementary Figure 16. Biotransformation of (-)-AuNPs in the endosomes/lysosomes of proximal tubules at 24h post intravenous injection. Representative EM images showing the biotransformation of (-)-AuNPs into gold nanoassemblies of nanofibers. Representative images are presented out of images acquired from 3 independent samples.

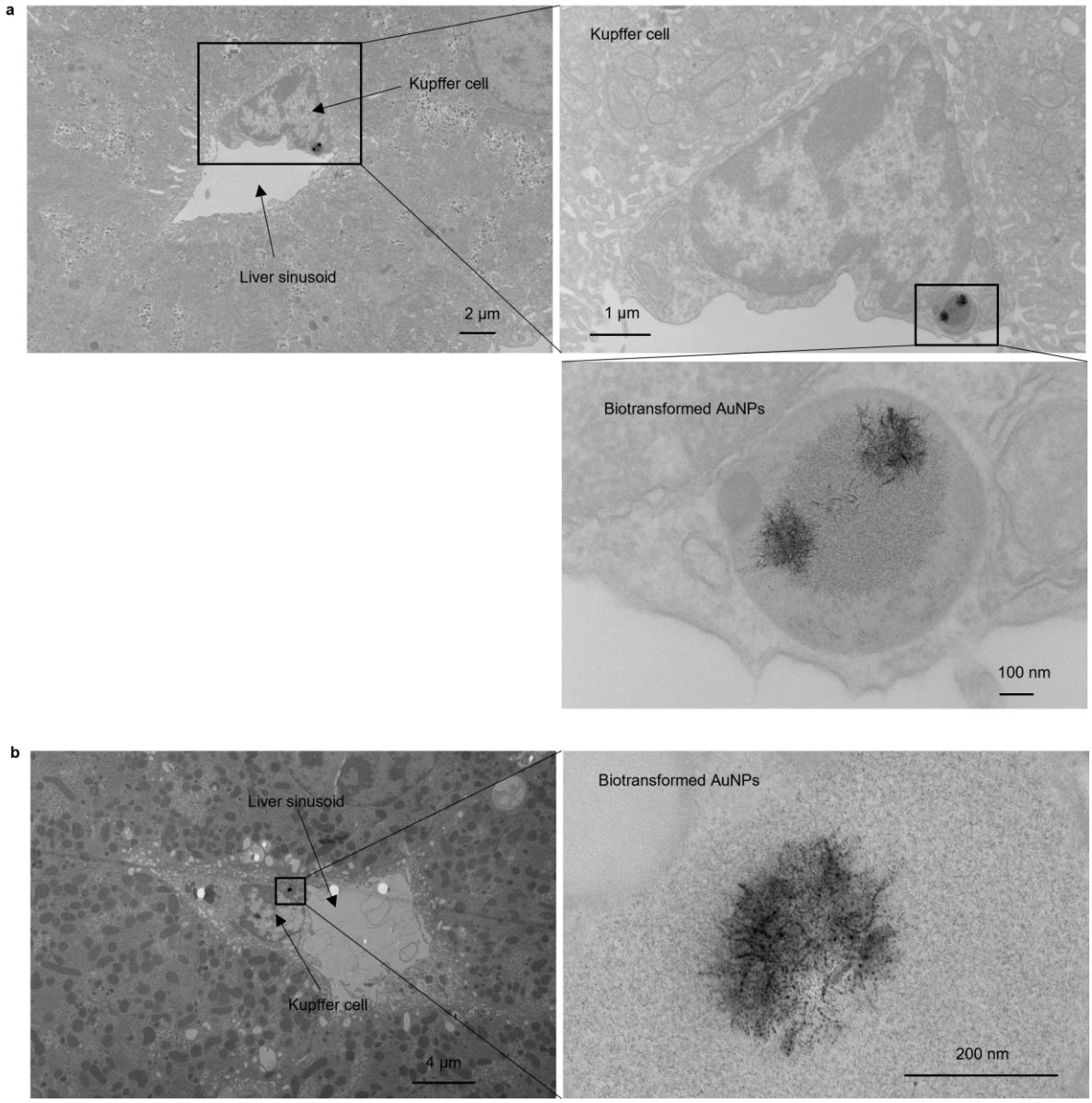

Supplementary Figure 17. Endocytosis and biotransformation of the (+)-AuNPs in Kupffer cells in the liver at 24h post intravenous injection. a and b, EM images showing the endocytosis of the (+)-AuNPs in the lysosomes of the Kupffer cells in the liver sinusoids. Kupffer cells are resident macrophages in the liver sinusoidal blood vessels. Consistently, biotransformation of the (+)-AuNPs in the lysosomes into flower-like nanoassemblies was observed, indicating that the intracellular biotransformation is not limited to the proximal tubular epithelial cells but can also occur in other cells such as macrophages. Representative images are presented out of images acquired from 3 independent samples.

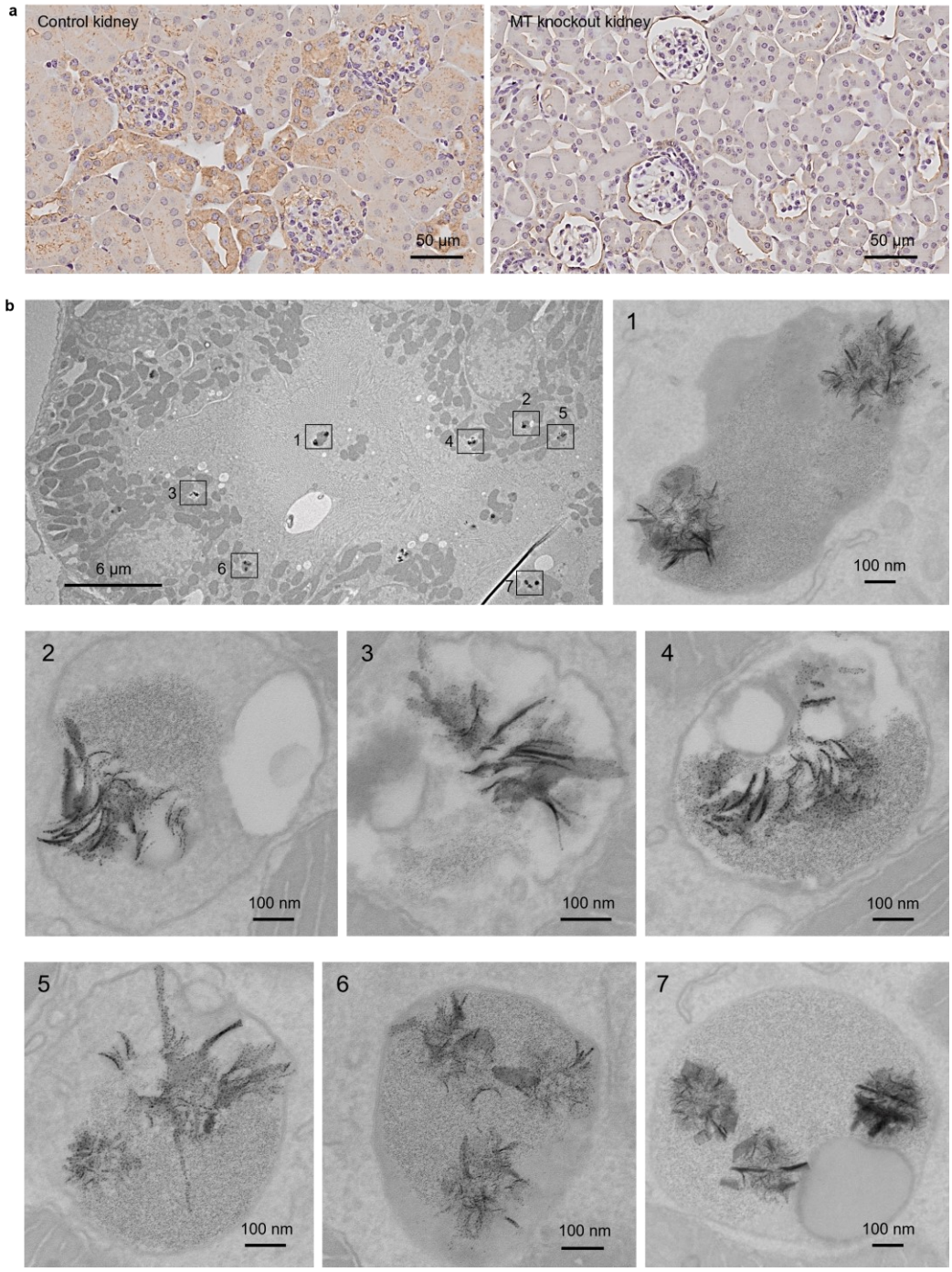

Supplementary Figure 18. Biotransformation of the (+)-AuNPs in metallothionein knock-out kidney. a, Immunohistochemical staining of metallothionein in tissue sections of the control kidneys and the metallothionein knock-out kidneys. The expression of metallothionein in metallothionein knock-out kidneys is significantly reduced. **b**, Representative EM images of proximal tubules in metallothionein knock-out kidneys. Biotransformation of endocytosed (+)-AuNPs to the typical flower-like nanoassemblies was consistently observed, indicating that metallothionein is not essential to the intracellular biotransformation of AuNPs. Representative images are presented out of images acquired from 3 independent samples.

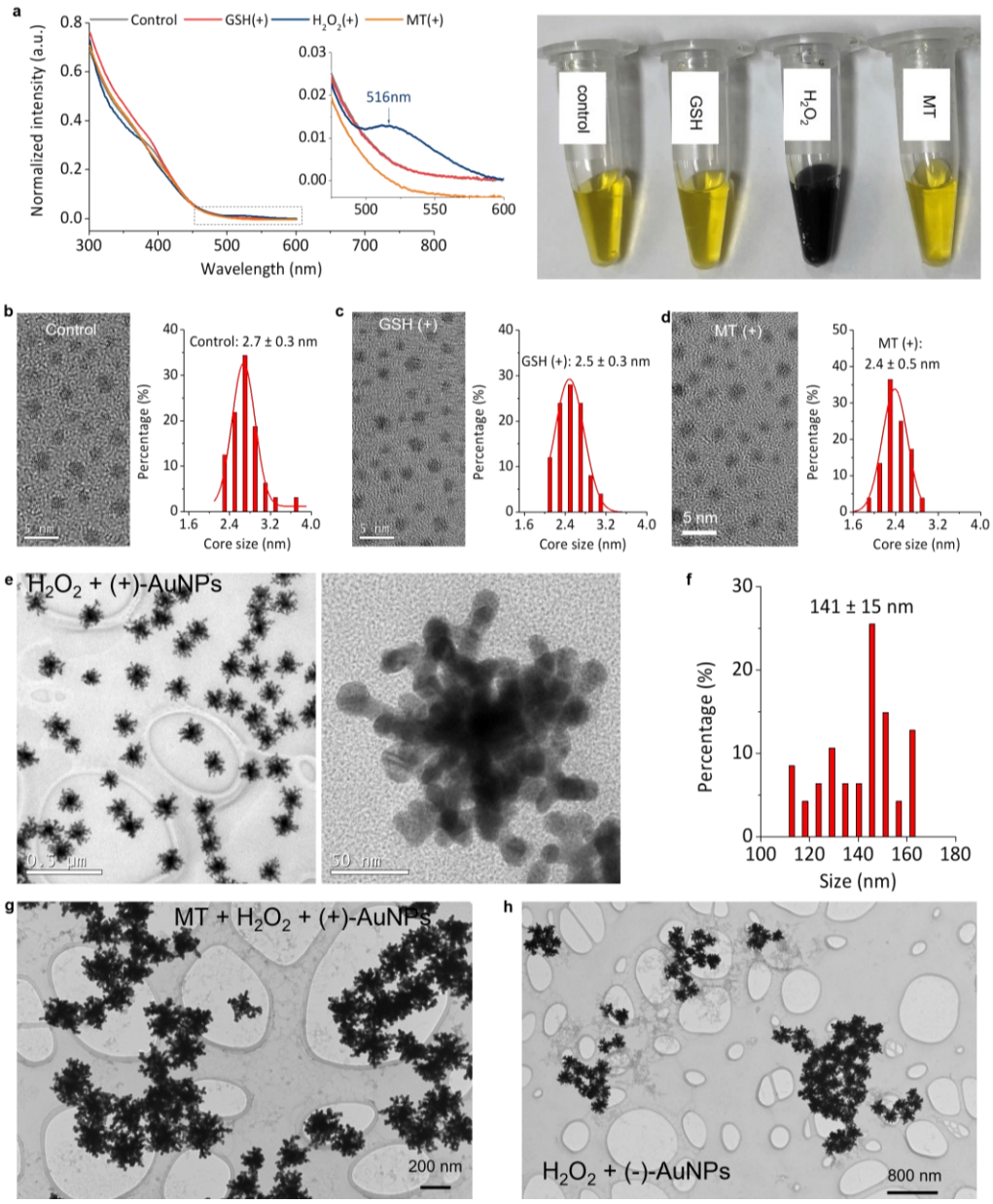

Supplementary Figure 19. Reactive oxygen species play a critical role in the intracellular biotransformation of AuNPs. a, Absorption spectra of the (+)-AuNPs after incubation with glutathione (GSH), metallothionein (MT) and H_2O_2 at pH 4.5 and room temperature for 24 h (left) and a photo showing the (+)-AuNPs solutions after incubation (right). A typical surface plasmon resonance peak at 516 nm was observed after incubation with H_2O_2 and the color of the (+)-AuNPs solution became dark, both indicating the formation of big gold nanostructures. **b to d,** Representative EM images and size quantification of the (+)-AuNPs after incubation with control PBS, GSH and MT, respectively. No significant change to the morphology and size of the (+)-AuNPs was observed after incubation with GSH and MT, indicating GSH and MT are not involved in the biotransformation of the (+)-AuNPs. **e and f,** Representative EM images and size quantification of the (+)-AuNPs after incubation with H_2O_2. Interestingly, dendritic gold nanoassemblies consisting of around 10nm gold aggregates were formed after incubation, which showed similar morphology to the flower-like gold nanoassemblies observed in vivo, suggesting that ROS may play a critical role in the intracellular biotransformation of AuNPs. **g,** Representative EM images of the (+)-AuNPs after incubation with MT and H_2O_2. MT didn't affect the formation of the dendritic gold nanoassemblies. **h,** Representative EM images of the (-)-AuNPs after incubation with MT and H_2O_2. H_2O_2 can also destabilize and induce the aggregation of the (-)-AuNPs. Experiments are repeated for at least 2 times with similar results.

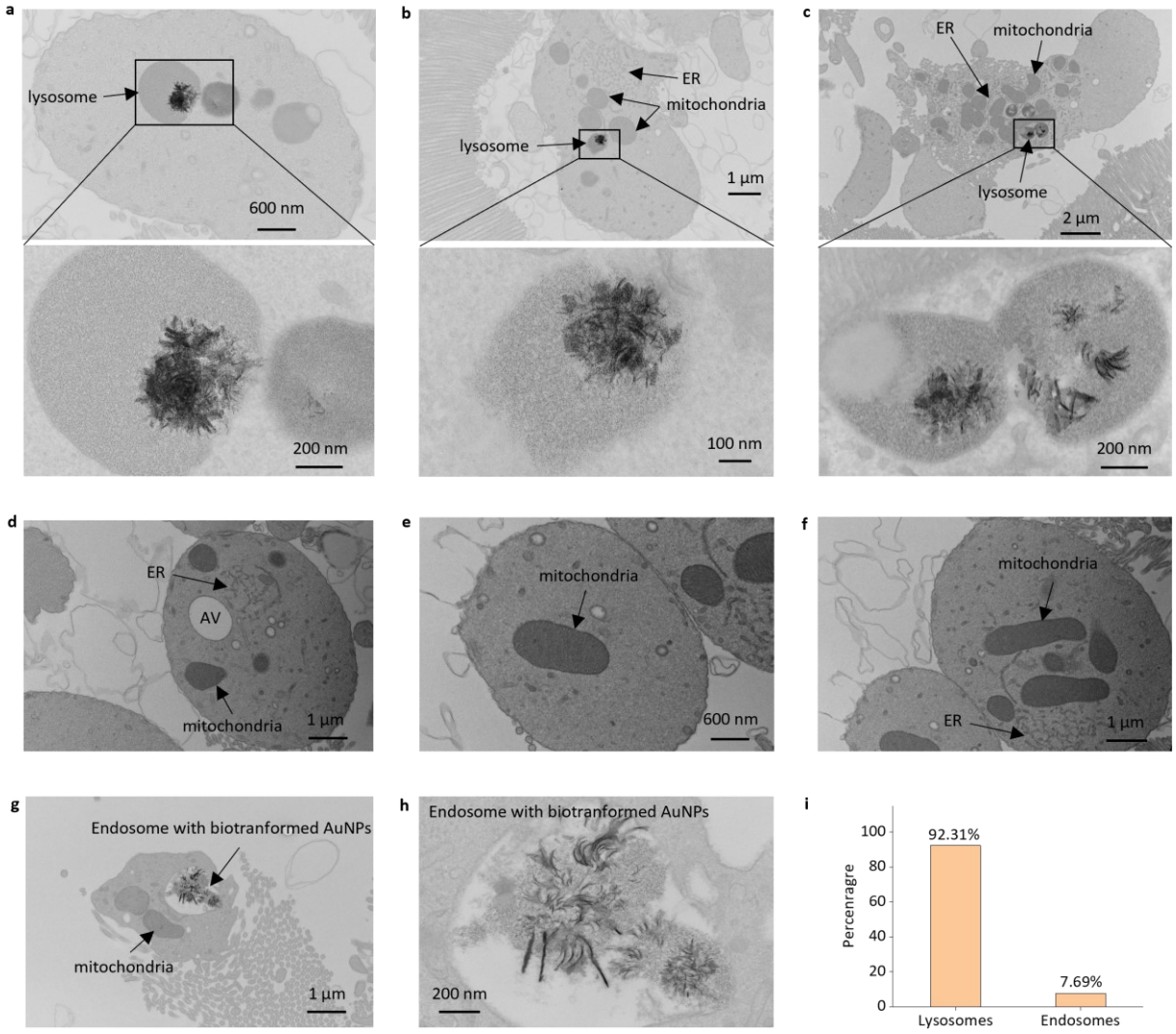

Supplementary Figure 20. Extracellular vesicles in proximal tubular lumen at 24h post intravenous injection of (+)-AuNPs. a to c, Representative EM images of extracellular vesicles (upper) containing lysosome-encapsulating biotransformed AuNPs (lower) in proximal tubular lumen. Other organelles including mitochondria and endoplasmic reticulum (ER) are also observed in the extracellular vesicles. **d to f**, Representative EM images of extracellular vesicles without the AuNPs but containing other organelles such as mitochondria, ER and apical vacuoles (AV) in proximal tubular lumen. **g**, A representative EM image showing biotransformed AuNPs in an endosome inside the extracellular vesicle. **h**, Magnified EM image of the endosome with biotransformed AuNPs in g. **i**, Quantification of the percentage of AuNPs in lysosomes and endosomes encapsulated in the extracellular vesicles. We analyzed 13 AuNP-containing vesicles inside the extracellular vesicles in proximal tubular lumen and found 12 AuNP-containing vesicles were lysosomes (92.31%) and one AuNP-containing vesicle was endosomes (7.69%). Representative images are presented out of images acquired from 3 independent samples.

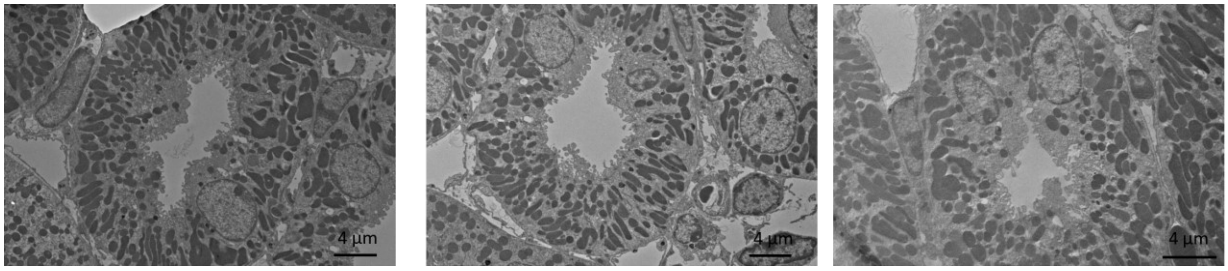

Supplementary Figure 21. Representative EM images of distal tubules at 24h post intravenous injection of (+)-AuNPs. There are no microvilli on the luminal side of distal tubules, different from proximal tubules. (+)-AuNPs were barely observed in distal tubules, indicating that distal tubules were not involved in the uptake of the AuNPs. Representative images are presented out of images acquired from 3 independent samples.

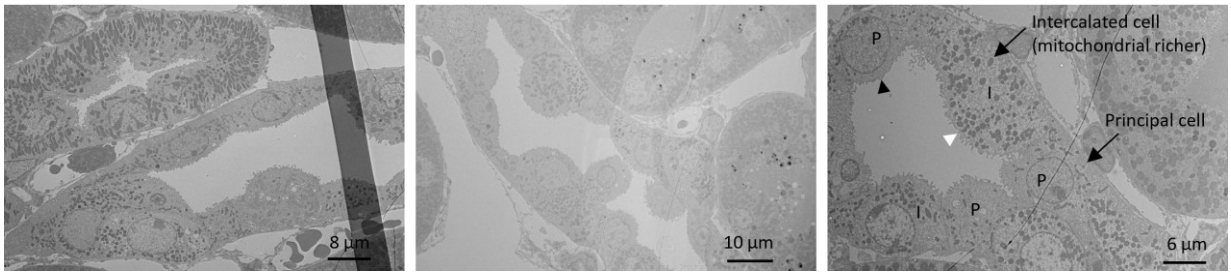

Supplementary Figure 22. Representative EM images of collecting ducts at 24h post intravenous injection of (+)-AuNPs. Collecting ducts consist of two types of epithelial cells: intercalated cells (labelled with I) and principal cells (labelled with P). Intercalated cells are mitochondrial richer than principal cells and are therefore electron-denser than principal cells under EM imaging. In addition, the apical membrane of principal cells (indicated by black triangle) is smoother than that of principal cells (indicated by white triangle). The AuNPs were not detected in both types of cells, implying that collecting ducts did not play a role in the uptake of the AuNPs. Representative images are presented out of images acquired from 3 independent samples.

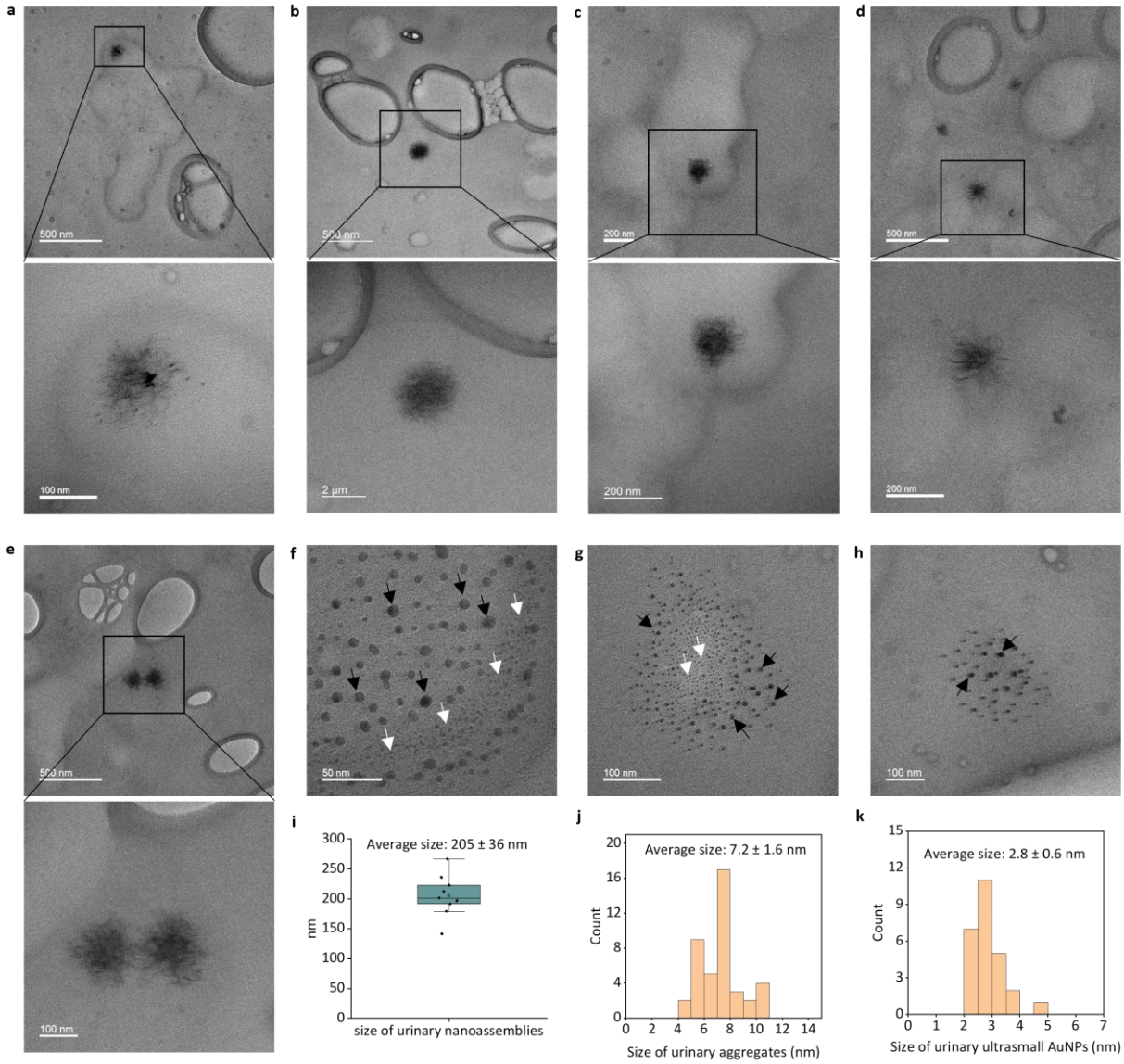

Supplementary Figure 23. The AuNPs with different morphologies in the urine collected within 24h post intravenous injection of (+)-AuNPs. a to e, Urinary flower-like biotransformed gold nanoassemblies. The lower images are magnified images of the gold nanoassemblies in the upper images. **f to h**, Urinary 5-10 nm AuNP aggregates (biotransformed AuNPs, labelled by black arrows) and ultrasmall (+)-AuNPs with original size of 2-3 nm (labelled by white arrows). **i**, Quantification of the average size of urinary gold nanoassemblies. The average size is 205 ± 36 nm (N = 9, mean ± s.d.), which is comparable to the sizes of the intracellular gold nanoassemblies (216 ± 55 nm, mean ± s.d., **Supplementary Figure 13d**). The box ranges from 25th percentiles (the first quartile, top of the boxes) to 75th percentiles (the third quartile, bottom of the boxes). The line in the box presents the median values. The whiskers are the lowest and highest points within 1.5 times the interquartile range of the lower and higher quartiles. **j**, Quantification of the average size of urinary AuNP aggregates by TEM. The size of urinary AuNP aggregates is 7.2 ± 1.6 nm, consistent with the average size of intracellular AuNP aggregates (7.5 ± 2.9 nm, **Supplementary Figure 13e**). **k**, Quantification of the average size of urinary ultrasmall AuNPs in the urine by TEM. Their average core size is 2.8 ± 0.6 nm, the same as the core size of synthesized (+)-AuNPs (2.7 ± 0.3 nm, **Supplementary Figure 1a**). Representative images are presented out of images acquired from 3 independent samples.

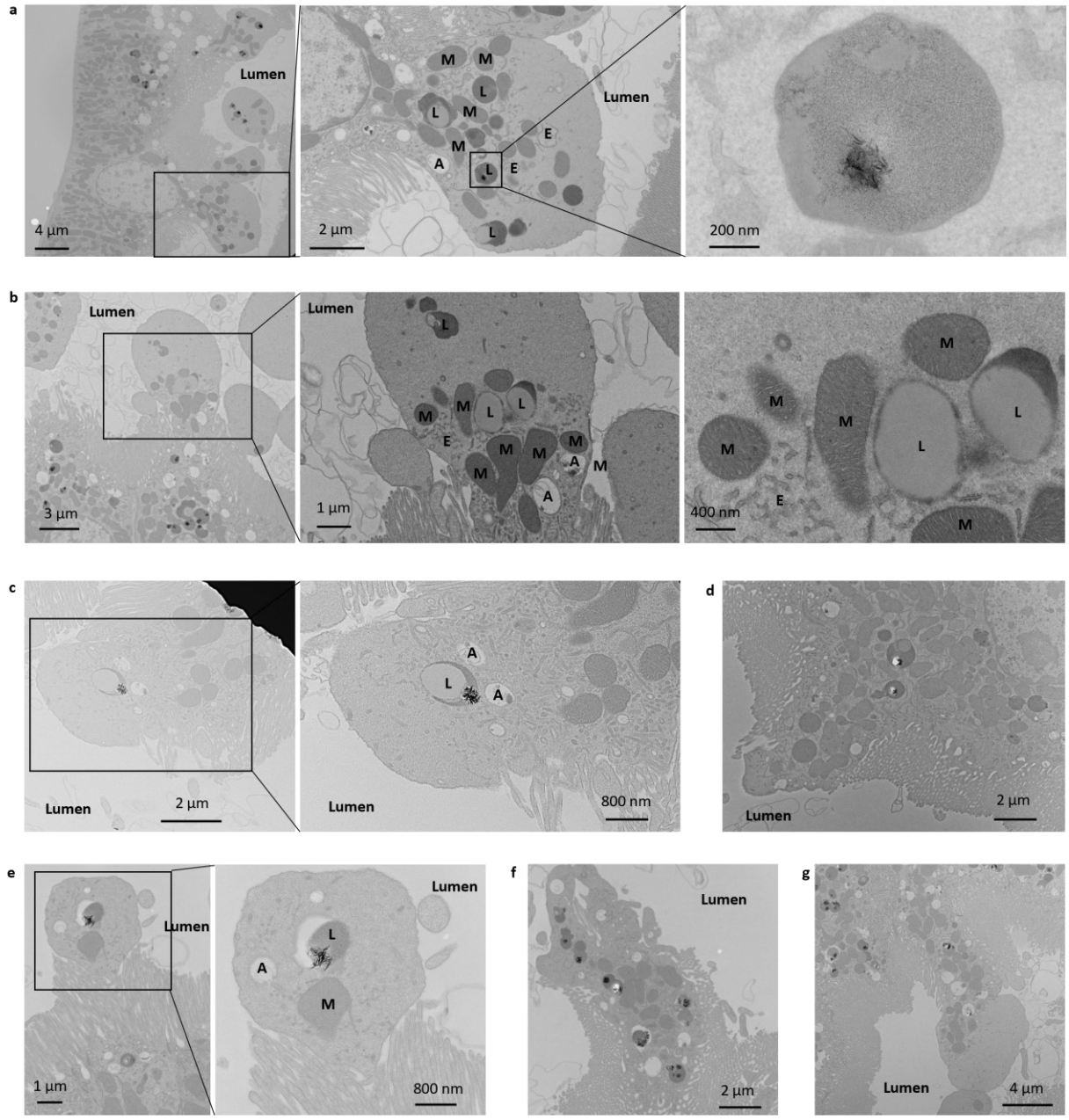

Supplementary Figure 24. Organelle extrusion of proximal tubular epithelial cells of the mice at 24h post intravenous injection of (+)-AuNPs. a to g, Representative EM images of organelle extrusion of proximal tubular epithelial cells. A fraction of cytoplasm was squeezed through the microvilli and extruded into the extracellular lumen space. Along with the extrusion of cytoplasm on the luminal membrane, lysosome (labelled as L) encapsulated AuNPs, mitochondria (labelled as M), apical vacuoles (labelled as A) and endoplasmic reticulum (labelled as E) were transported together into the extrusions on the luminal membrane. Representative images are presented out of images acquired from 3 independent samples.

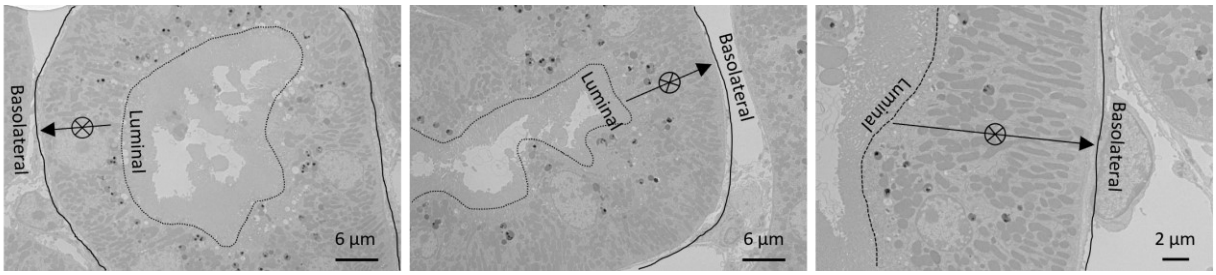

Supplementary Figure 25. Endocytosed (+)-AuNPs on the luminal side of proximal tubules were not reabsorbed back to blood circulation through tubular reabsorption. We did not observe the extrusion of cytoplasm on the basolateral side of PTECs. We did not observe the migration of endocytosed AuNPs on the luminal side (dash line) to the basolateral side (solid line) of the proximal tubules, indicating that endocytosed AuNPs would not be reabsorbed back into the blood stream from the basolateral side. Representative images are presented out of images acquired from 3 independent samples.

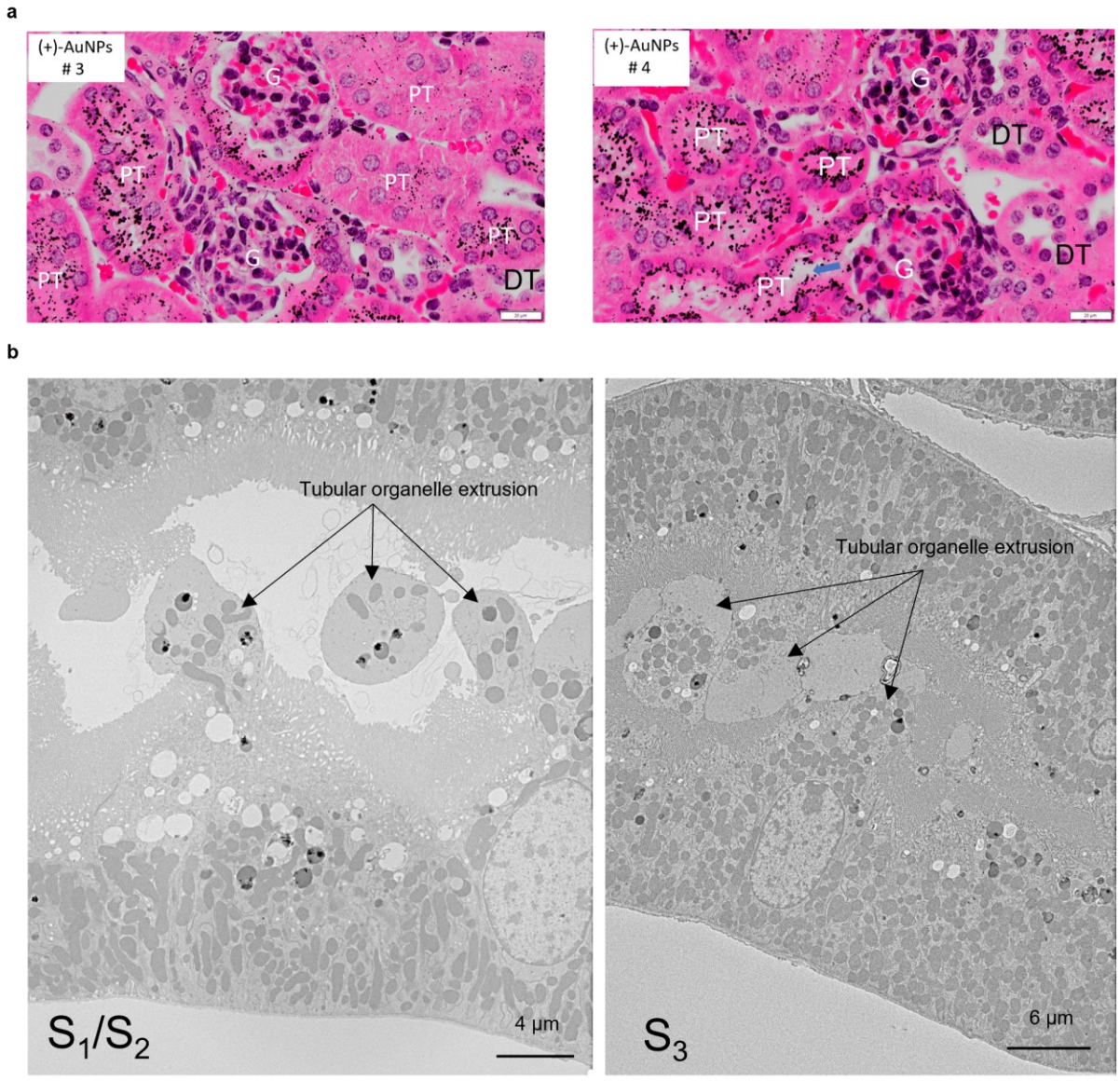

Supplementary Figure 26. a, Representative images of H&E-stained silver enhanced kidney tissue sections of normal mice showing distribution of (+)-AuNPs in the renal cortex at 24h post intravenous injection. The arrow points the part of S_1 segment of proximal tubule that is directly connected to the renal capsule., **b**, Representative EM images of S_1 or S_2 and S_3 segments of proximal tubules at 24 h post intravenous injection of (+)-AuNPs. Although it was challenging to differentiate S2 from S1 in EM images in our case due to their very similar brush boarder heights, mitochondrial conformation, and distribution, the S3 segments indeed can be identified based on their unique conformation of the mitochondria. Uptake of the (+)-AuNPs and membrane extrusion also occurred in S_3 segment of the proximal tubules in addition to S_1/S_2 segment. Representative images are presented out of images acquired from 3 independent samples.

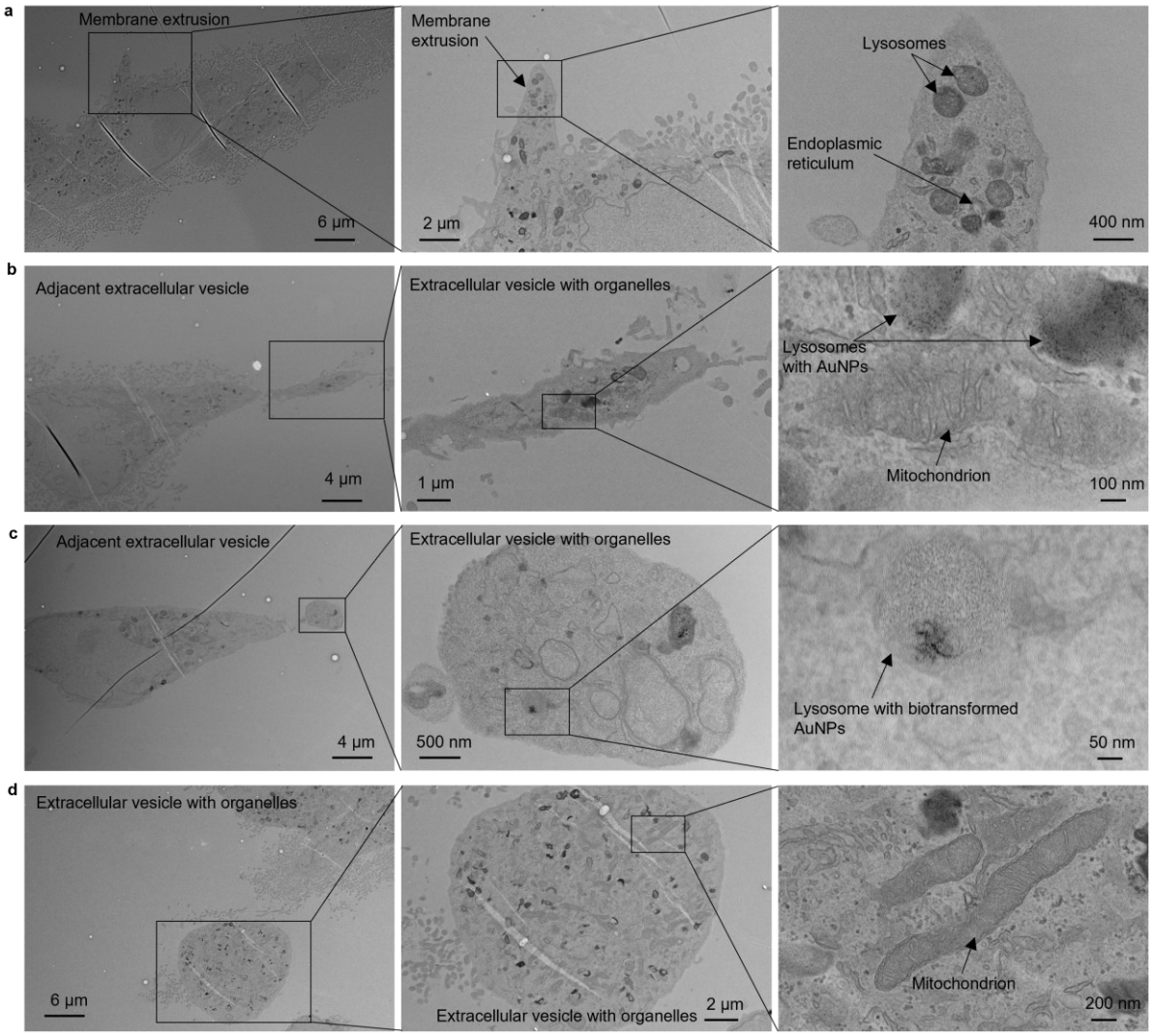

Supplementary Figure 27. Representative EM images of monolayer human kidney proximal tubular cells (HK-2) after incubation with the (+)-AuNPs overnight. a, HK-2 cell with membrane extrusion containing intracellular organelles including lysosomes and endoplasmic reticulum. **b**, HK-2 cells with adjacent extracellular vesicles containing intracellular organelles including mitochondria and lysosomes with AuNPs were also observed. **c**, HK-2 cells with adjacent extracellular vesicles containing intracellular organelles including mitochondria and lysosomes with biotransformed AuNPs were also observed. **d**, Extracellular vesicles containing intracellular organelles including mitochondria and lysosomes were observed. Representative images are presented out of images acquired from 3 independent samples.

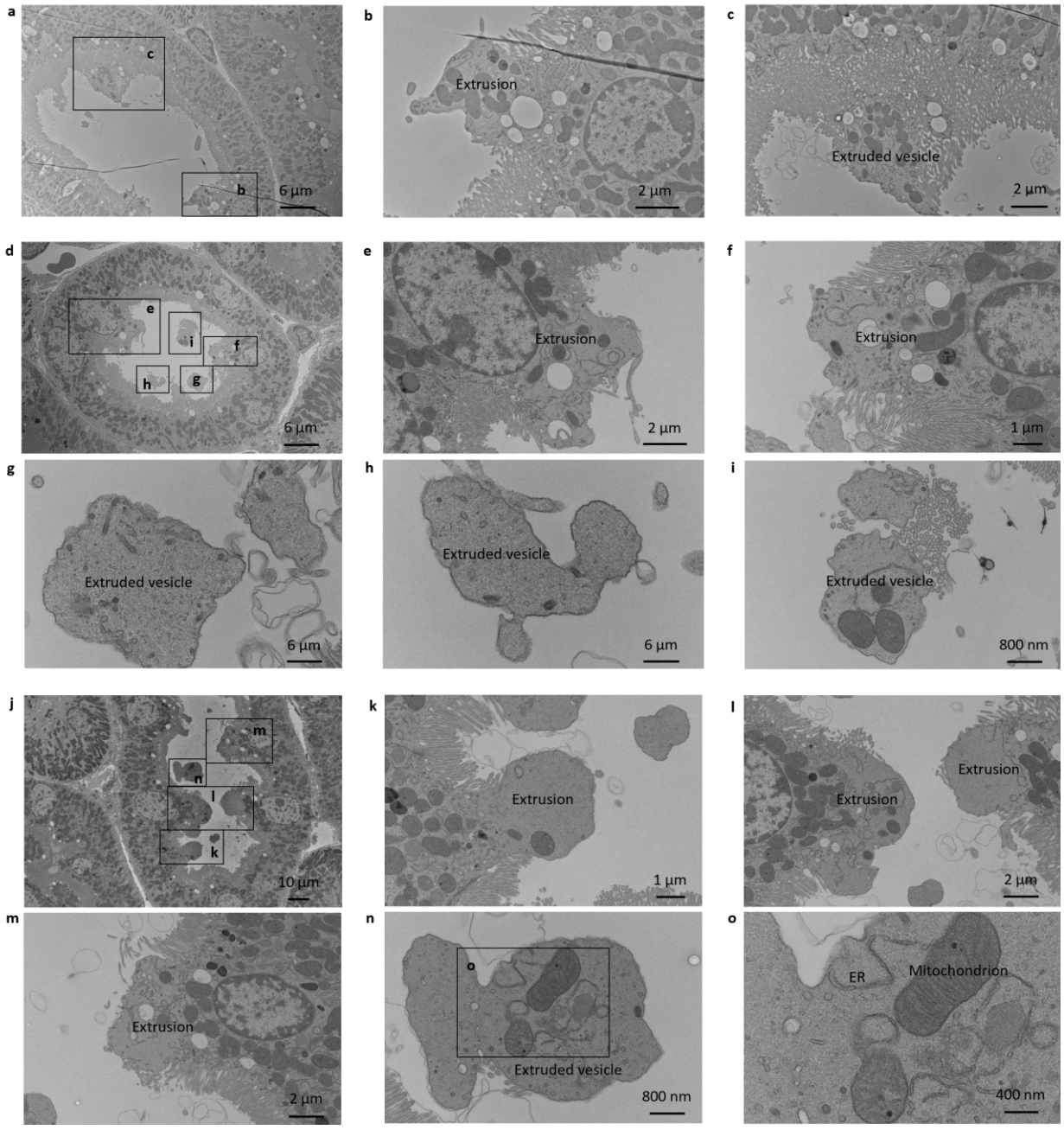

Supplementary Figure 28. Organelle extrusion of proximal tubular epithelial cells in PBS-injected mice. a, A representative EM images of proximal tubules. **b**, Magnified EM image of the extrusion on luminal membrane in **a**. **c**, Magnified EM image of the extruded vesicle in **a**. **d**, A representative EM images of proximal tubules. **e and f**, Magnified EM images of the extrusions on luminal membrane in **d**. **g to i**, Magnified EM images of the extruded vesicles in lumen in **d**. **j**, A representative EM images of proximal tubules. **k to m**, Magnified EM images of the extrusions in **j**. **n**, Magnified EM image of the extruded vesicle in **j**. **o**, Magnified EM image of the organelles including mitochondria and ER in the extruded vesicle in **n**. Representative images are presented out of images acquired from 3 independent samples.

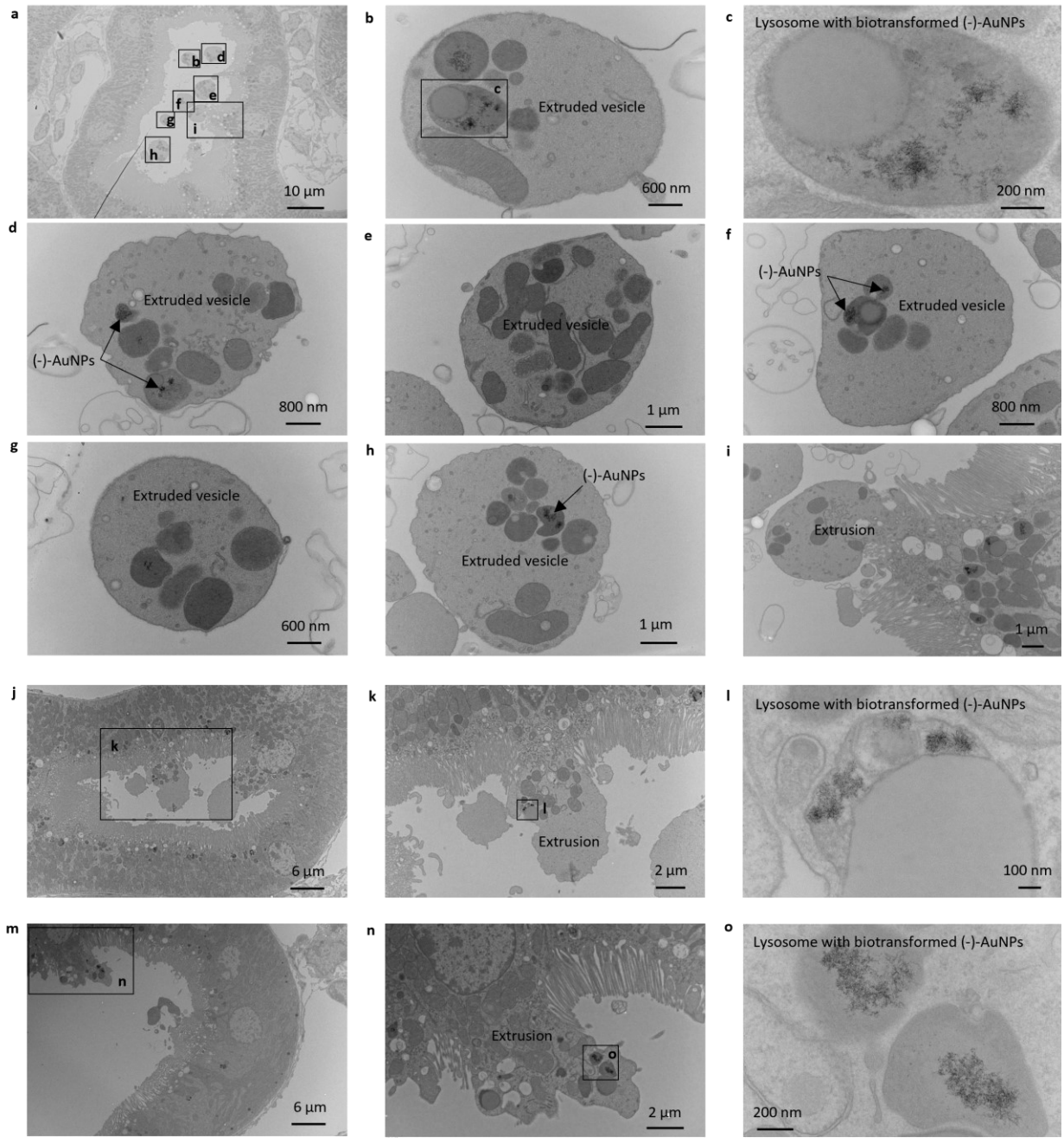

Supplementary Figure 29. Organelle extrusion of proximal tubular epithelial cells in (-)-AuNPs-injected mice. a, A representative EM images of proximal tubules. **b**, Magnified EM image of the extruded vesicle in **a**. **c**, Magnified EM image of a lysosome with biotransformed (-)-AuNPs in the extruded vesicle in **b**. **d to h**, Magnified EM images of the extruded vesicles in **a**. **i**, Magnified EM images of the extrusions in **a**. **j**, A representative EM images of proximal tubules. **k**, Magnified EM images of the extrusion in **j**. **l**, Magnified EM image of a lysosome with biotransformed (-)-AuNPs in the extrusion in **j**. **m**, A representative EM images of proximal tubules. **n**, Magnified EM image of the extrusion in **m**. **o**, Magnified EM image of a lysosome with biotransformed (-)-AuNPs in the extrusion in **n**. Representative images are presented out of images acquired from 3 independent samples.

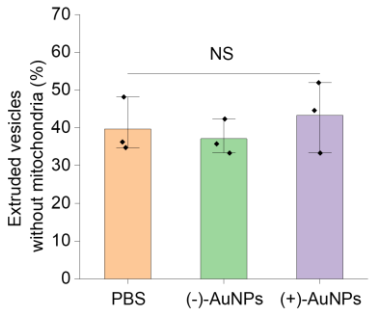

Supplementary Figure 30. Quantification of the percentage of extruded vesicles without mitochondria in PBS, (-)-AuNPs and (+)-AuNPs-injected mice. N = 3 tissue sections from 3 individual tissue blocks, mean ± s.d. We analyzed more than 70 extruded vesicles in EM images of each tissue section for PBS, (-)-AuNPs and (+)-AuNPs-injected mice, respectively. $p = 0.61$. Data are presented as mean ± s.d.. Data are analyzed using one-way ANOVA at the 0.05 significance level. NS, no significant difference.

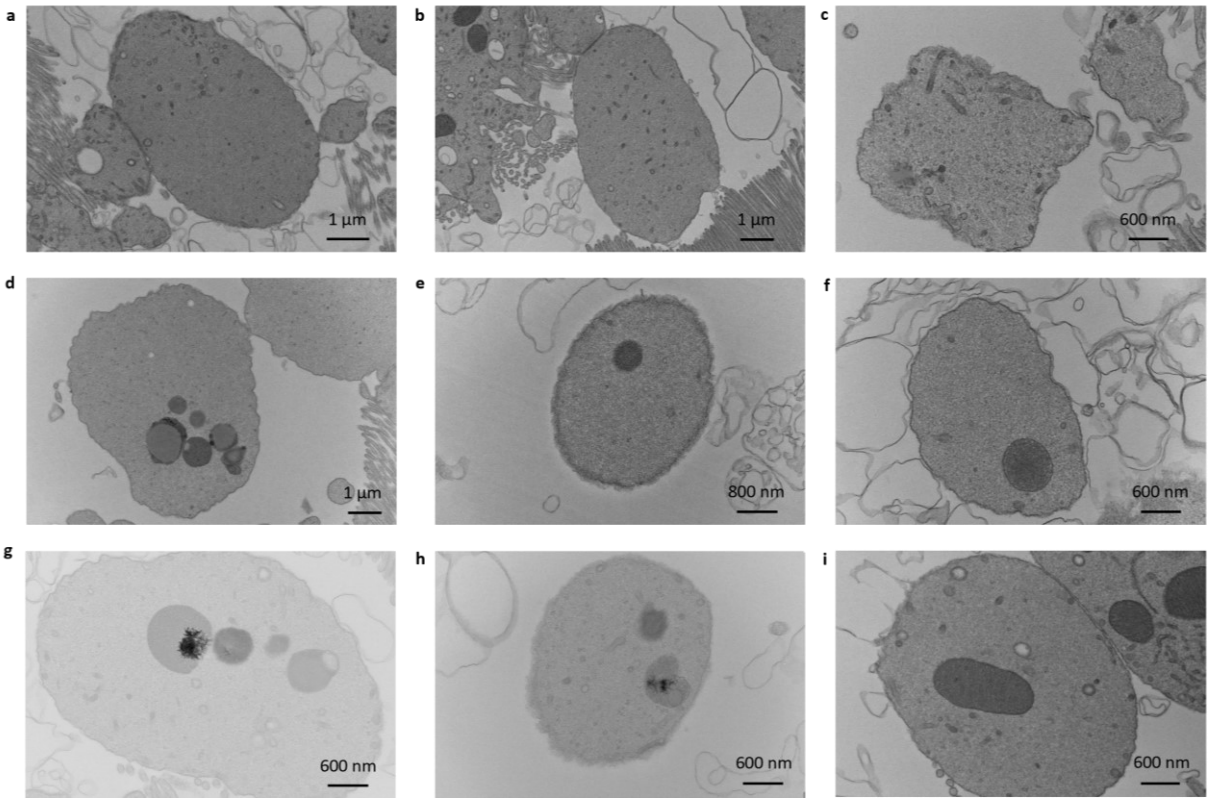

Supplementary Figure 31. Extruded vesicles containing different types of organelles. a to c, Representative EM images of extruded vesicles with neither mitochondria nor lysosomes. **d to h**, Representative EM images of the extruded vesicles with only lysosomes. **i**, A representative EM image of extruded vesicles with only mitochondria. Together these images indicate that the organelle extrusion is not specific to removal of a certain type of organelles. Representative images are presented out of images acquired from 3 independent samples.

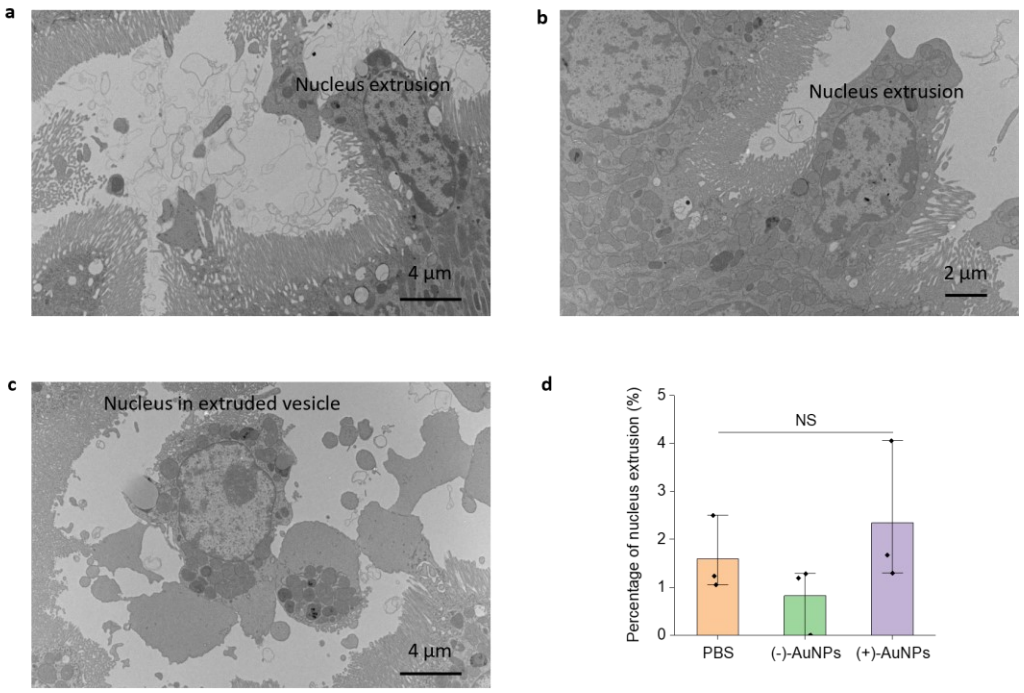

Supplementary Figure 32. Extrusion of a nucleus. a and b, Representative EM images of extrusion of nucleus. **c**, A representative EM image of a nucleus in an extruded vesicle. **d**, Quantification of the percentage of nucleus extrusion in PBS, (-)-AuNPs and (+)-AuNPs-treated groups. The percentage in each group is below 3%, indicating the low frequency of nucleus extrusion in proximal tubules. N = 3 tissue sections from 3 individual tissue blocks, mean ± s.d. We analyzed more than 70 cross sections of proximal tubules in EM images of each tissue section for PBS, (-)-AuNPs and (+)-AuNPs-injected mice, respectively. $p = 0.29$. Data are presented as mean ± s.d.. Data are analyzed using one-way ANOVA at the 0.05 significance level. NS, no significant difference.

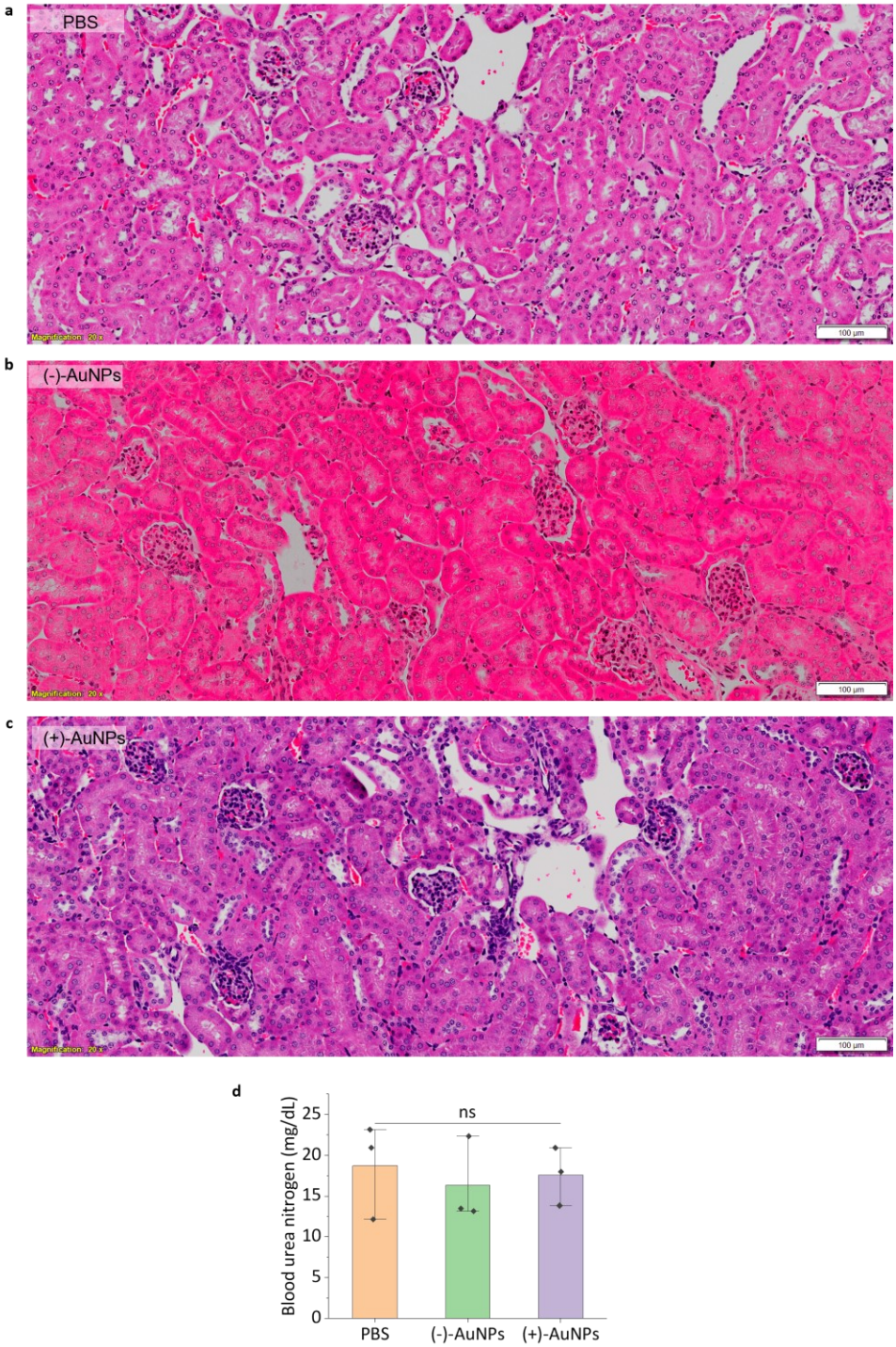

Supplementary Figure 33. Renal pathology and renal function biomarker level of the mice at 24h post intravenous injection of PBS, (-)-AuNPs and (+)-AuNPs. a to c, Representative images of renal pathology in PBS (**a**), (-)-AuNPs (**b**) and (+)-AuNPs (**c**) groups. The structure of renal tissue remained healthy, and no obvious pathological damage was observed in all groups, indicating that injection of AuNPs caused no renal damage. **d**, Blood urea nitrogen levels were comparable in PBS, (-)-AuNPs and (+)-AuNPs-injected mice (N = 3 mice for each group, mean ± s.d.), further proving that injection of AuNPs didn't affect the renal functions. $p = 0.84$. Data are presented as mean ± s.d.. Data are analyzed using one-way ANOVA at the 0.05 significance level. NS, no significant difference.

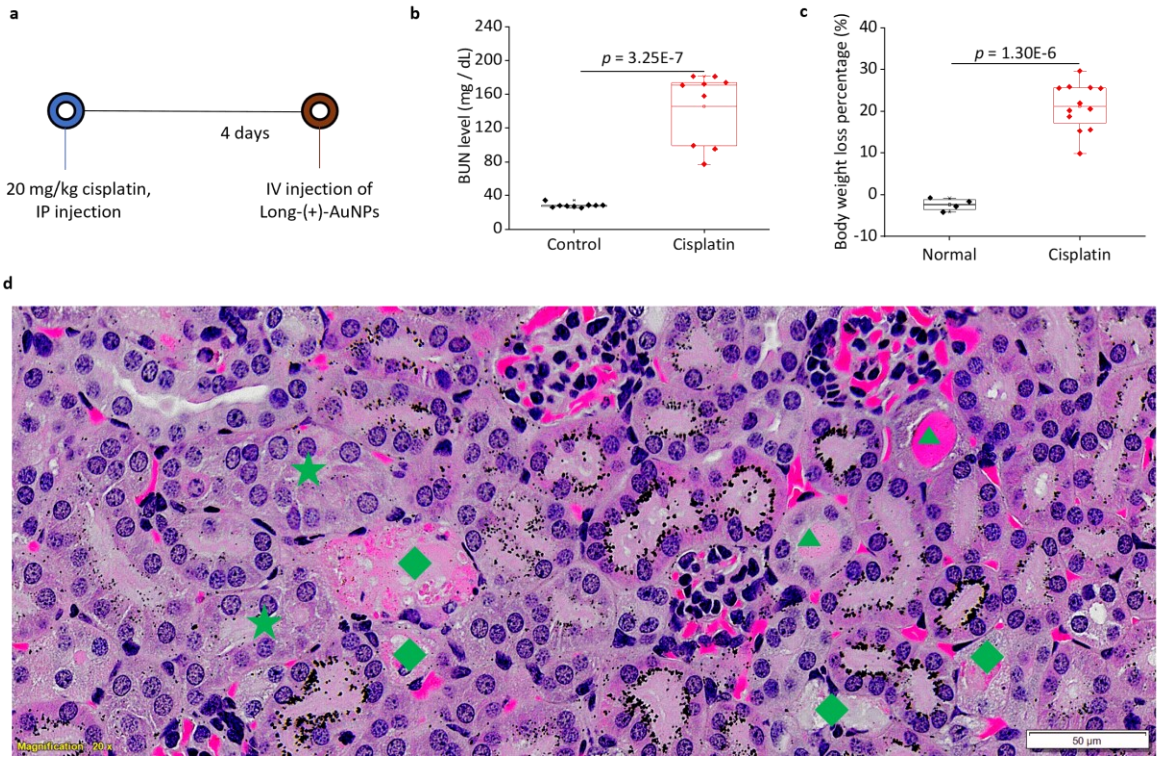

Supplementary Figure 34. Establishment and characterizations of cisplatin-induced proximal tubular injury model. a, Establishment of the model. Cisplatin was intraperitoneally injected into the abdominal cavity of mice at a dose of 20 mg/kg body weight. After four days, the body weight of mice was measured, and the blood samples of mice were collected from the venous sinus. Meanwhile, (+)-AuNPs are intravenously injected into mice. At 24h post injection of (+)-AuNPs, mice were sacrificed to harvest the kidneys for tissue imaging and pathology analysis. **b**, Blood urea nitrogen level was significantly elevated in cisplatin-treated mice 4 days after cisplatin administration, indicating loss of kidney function. N = 10 mice for each group. **c**, Body weight of cisplatin-treated mice decreased by ~20% in 4 days post cisplatin injection (N = 12), in contrast to the ~2% increase in body weight of normal mice (N = 4). The boxes in **b** and **c** range from 25th percentiles (the first quartile, top of the boxes) to 75th percentiles (the third quartile, bottom of the boxes). The lines in the boxes present the median values. The whiskers are the lowest and highest points within 1.5 times the interquartile range of the lower and higher quartiles. Two-sided Student`s t-test was performed at the 0.05 significance level. **d**, Renal pathology showed obvious heterogeneous focal damage to the proximal tubules in cisplatin-treated mice. Intracellular vacuolization (labelled by green stars), protein cast (labelled by green triangles) and degenerated proximal tubules (labelled by green diamonds) were observed, while normal proximal tubules with AuNPs uptake (black dots, visualized by silver enhancement) also existed.

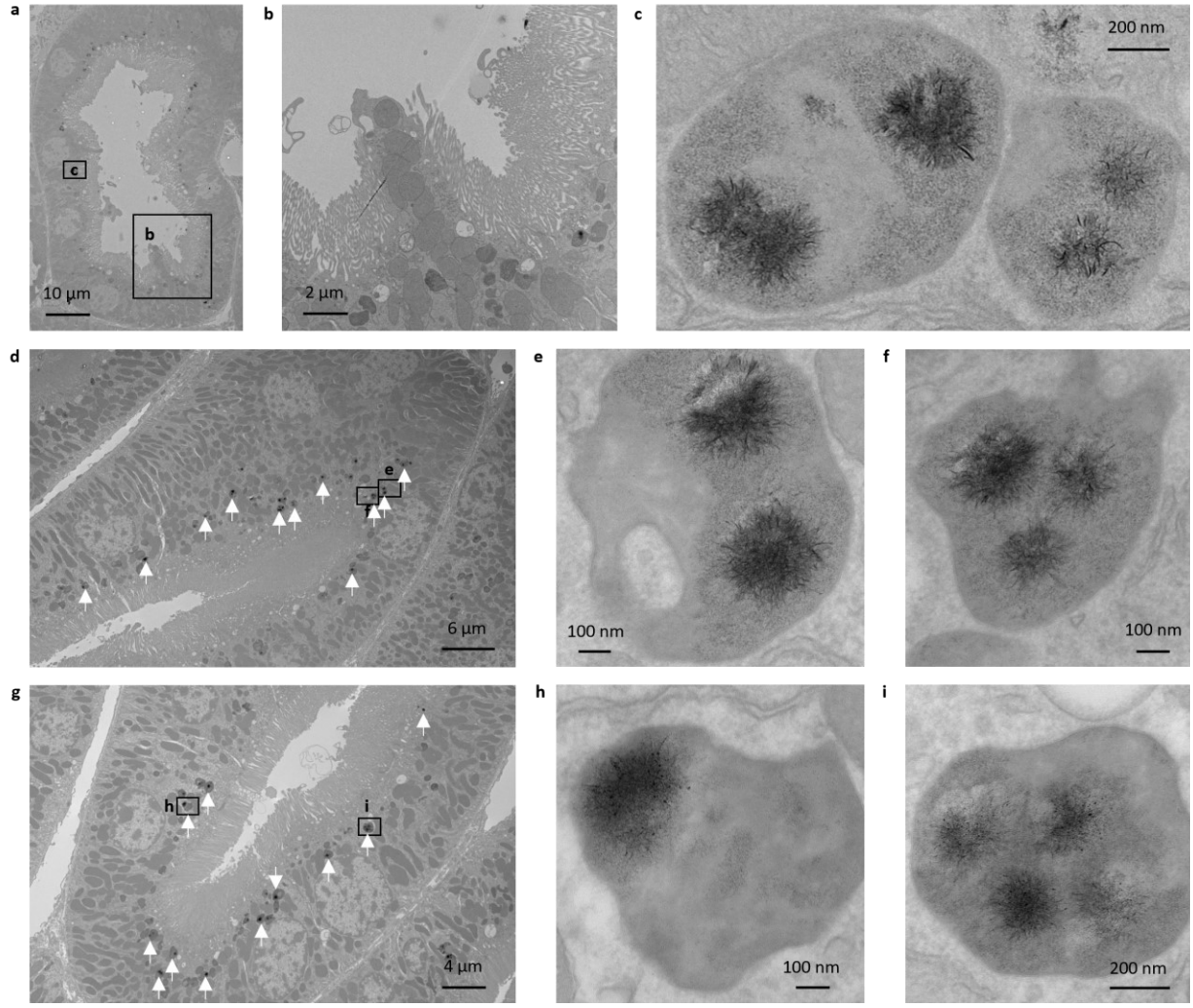

Supplementary Figure 35. Extrusion and biotransformation in proximal tubules with appearing normal morphology in mouse model of cisplatin-induced acute tubular injury at 24h post intravenous injection of (+)-AuNPs. a, A representative EM image of normal proximal tubules. **b**, Magnified EM image of the extrusion in **a**. **c**, Magnified EM image of biotransformed (+)-AuNPs in lysosomes in **a**. **d**, A representative EM image of normal proximal tubules. **e and f**, Magnified EM images of biotransformed (+)-AuNPs in lysosomes in **d**. **g**, A representative EM image of normal proximal tubules. **h and i**, Magnified EM images of biotransformed (+)-AuNPs in lysosomes in **g**. Representative images are presented out of images acquired from 3 independent samples.

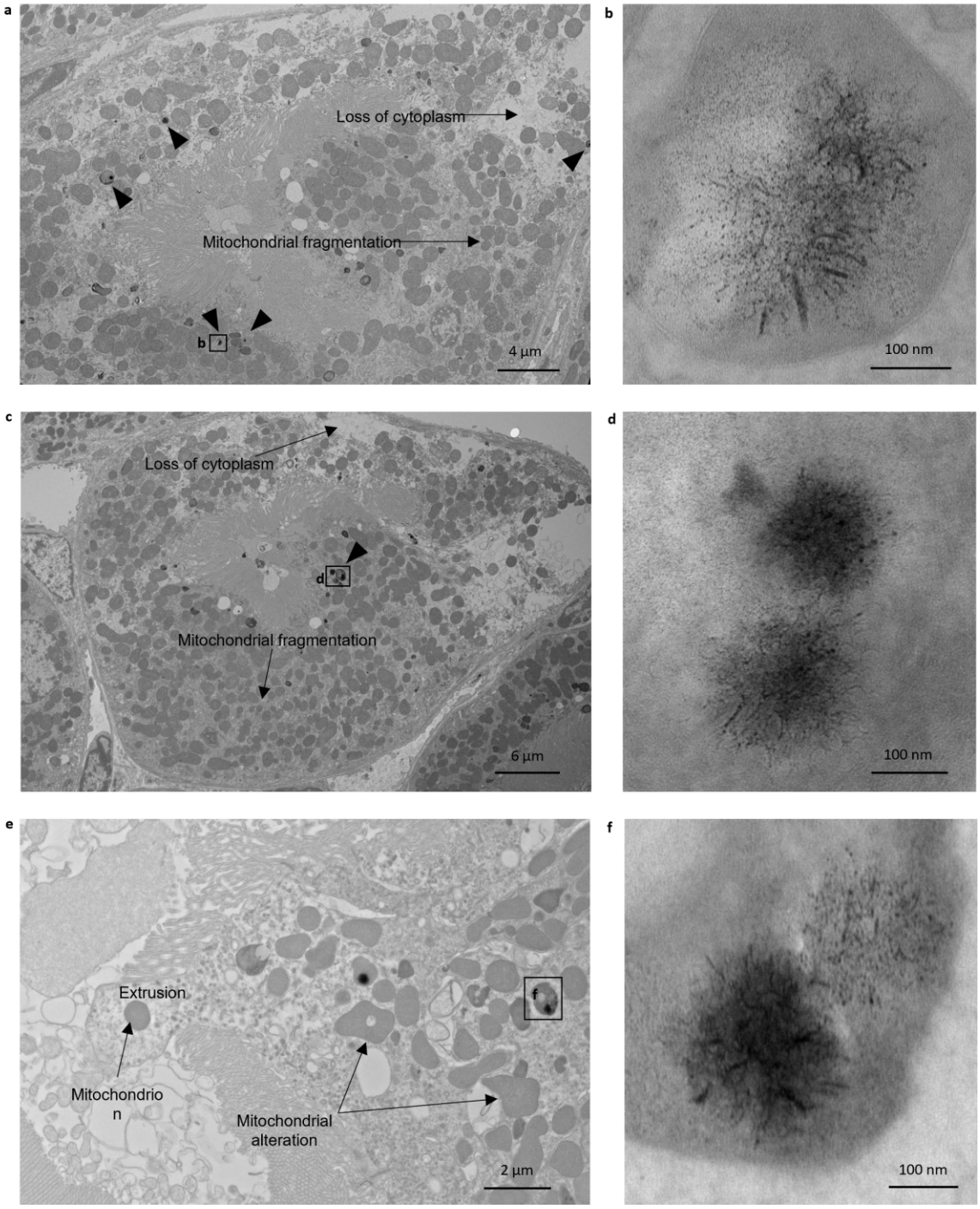

Supplementary Figure 36. Extrusion and biotransformation in mildly damaged proximal tubules in mouse model of cisplatin-induced acute tubular injury at 24h post intravenous injection of (+)-AuNPs. a and c, Representative EM images of mildly damaged proximal tubules. Loss of cytoplasm and mitochondrial fragmentation were observed. **b and d**, Magnified EM images of biotransformed (+)-AuNPs in **a and c**, respectively. **e**, A representative EM image of mildly damaged proximal tubules with extrusion. Mitochondrial alteration was observed. The contrast of cytoplasm decreased due to loss of cytoplasm content. **f**, Magnified EM image of biotransformed (+)-AuNPs in lysosomes in **e**. Together these images indicate that biotransformation of the AuNPs was not affected in mildly damaged proximal tubules. Representative images are presented out of images acquired from 3 independent samples.

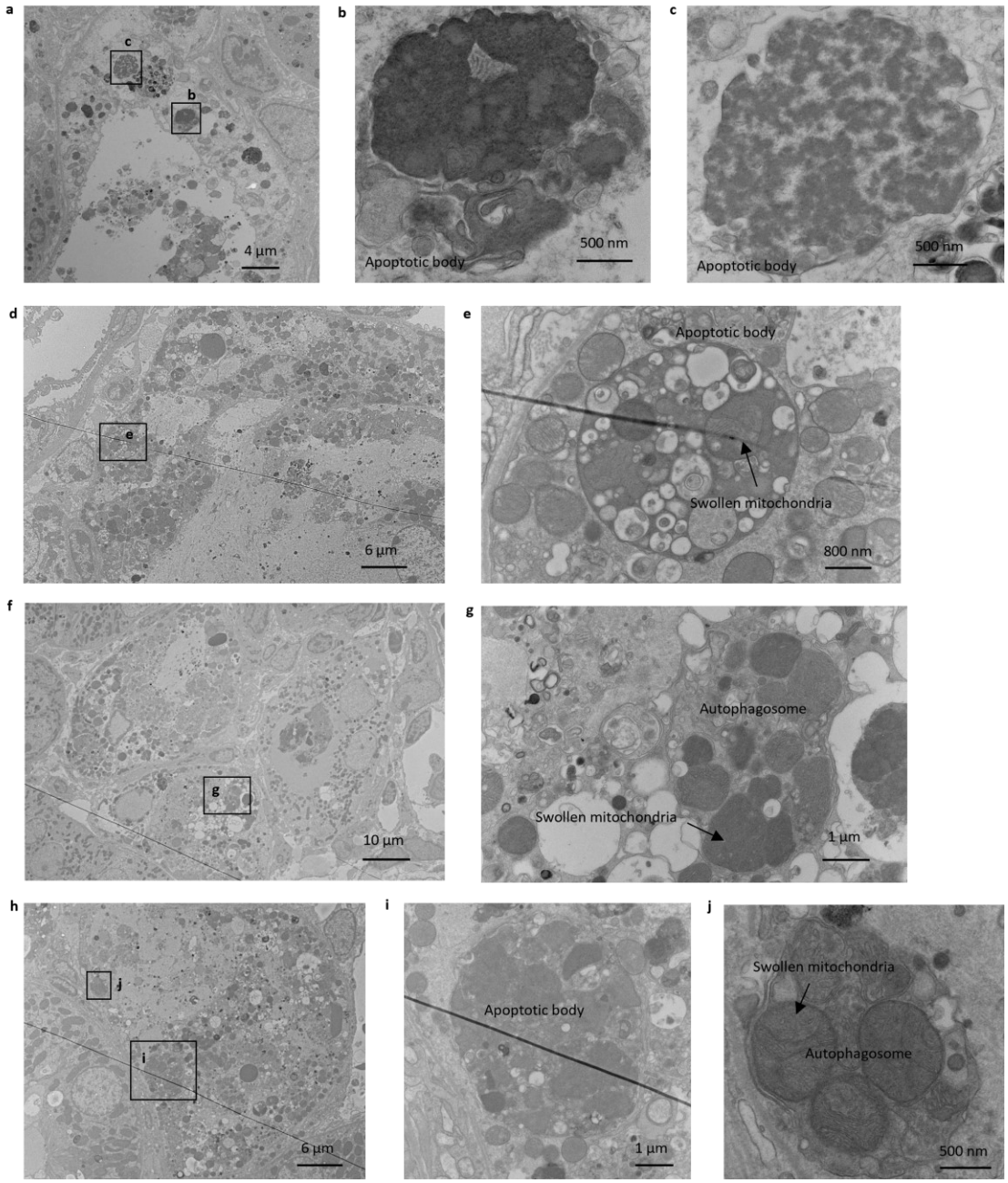

Supplementary Figure 37. Autophagosomes and apoptotic bodies in severely damaged proximal tubules in mouse model of cisplatin-induced acute tubular injury at 24h post intravenous injection of (+)-AuNPs. a, A representative EM image of severely damaged proximal tubule. The AuNPs were barely observed in severely damaged proximal tubules due to degenerated cell structures. Autophagosomes and apoptotic bodies were observed. **b and c**, Magnified EM images of apoptotic bodies in **a**. **d**, A representative EM image of severely damaged proximal tubule. **e**, Magnified EM image of an apoptotic body in **a**. **f**, A representative EM image of severely damaged proximal tubule. **g**, Magnified EM image of an autophagosome in **f**. **h**, A representative EM image of severely damaged proximal tubule. **i**, Magnified EM image of an apoptotic body in **h**. **j**, Magnified EM image of an autophagosome in **h**. Autophagosomes have a smaller average size compared to apoptotic bodies and contain mostly swollen mitochondria, while apoptotic bodies have more complex contents. Both autophagosomes and apoptotic bodies showed distinct morphologies to extruded vesicles we observed in the normal conditions. Representative images are presented out of images acquired from 3 independent samples.

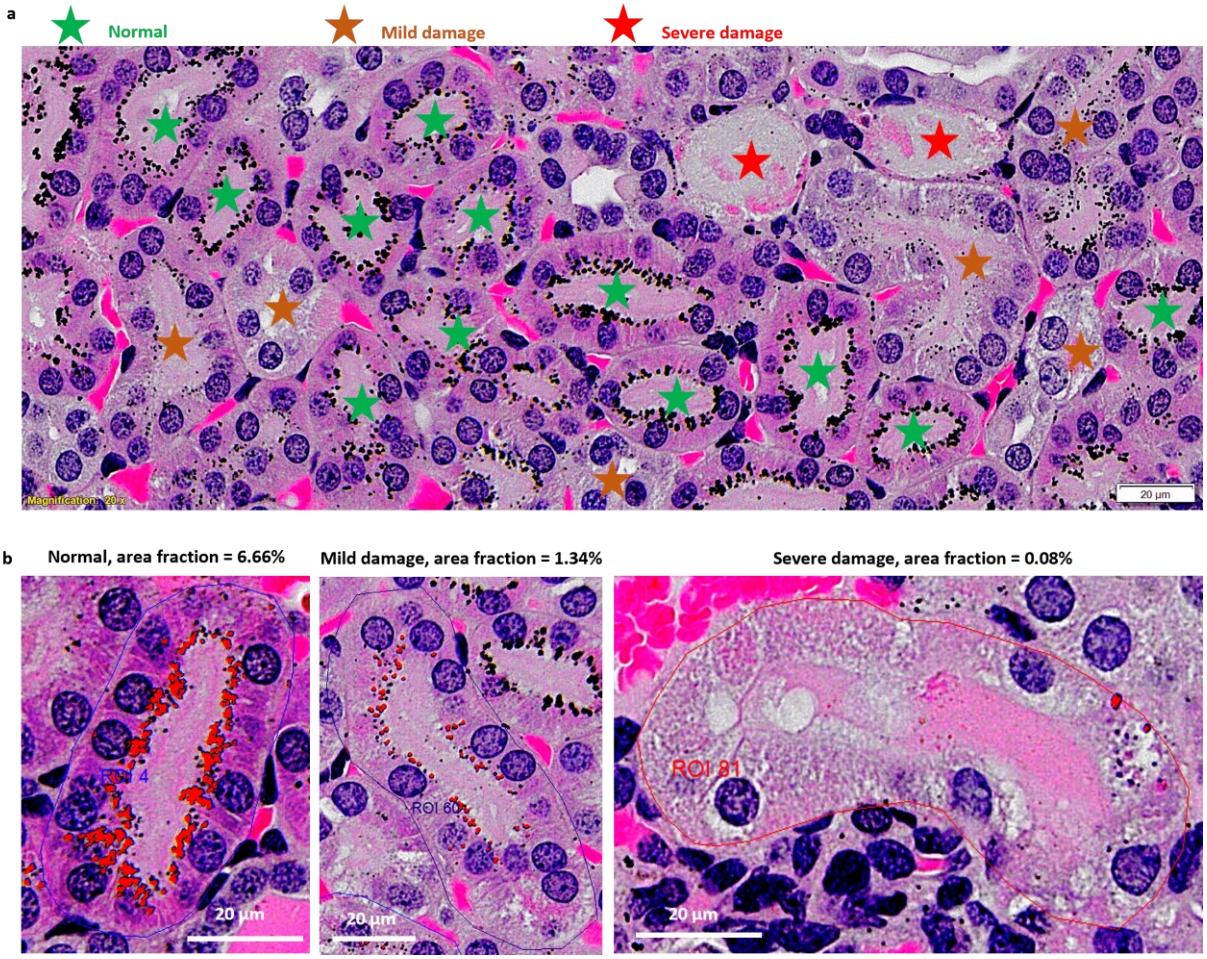

Supplementary Figure 38. Quantification of the uptake efficiencies of (+)-AuNPs in normal, mildly damaged and severely damaged proximal tubules. a, A representative H&E-stained and silver-enhanced kidney tissue section of the mouse model of cisplatin-induced acute tubular injury. The kidney was obtained at 24h post intravenous injection of (+)-AuNPs. Consistent with previous findings, the cisplatin induced heterogeneous focal tubular injury rather than diffusive damages. AuNPs were enhanced to black dots. Normal, mildly damaged and severely damaged proximal tubules are observed on the same kidney and labelled by green, orange and red stars, respectively. The uptake of AuNPs decreased with the progress of damage. **b**, Representative H&E-stained and silver-enhanced kidney tissue sections showing the quantification of area fraction of the AuNPs in proximal tubules at different damage stages based on the protocol shown in **Supplementary Figure 7**. Representative images are presented out of images acquired from 3 independent samples.

3. Supplementary references.

1. Klumperman, J. & Raposo, G.J.C.S.H.p.i.b. The complex ultrastructure of the endolysosomal system. **6**, a016857 (2014).
2. Zhuo, J.L. & Li, X.C. Proximal nephron. *Comprehensive Physiology* **3**, 1079-1123 (2013).
3. Liu, J. et al. PEGylation and Zwitterionization: Pros and Cons in the Renal Clearance and Tumor Targeting of Near-IR-Emitting Gold Nanoparticles. **52**, 12572-12576 (2013).
4. Peng, C. et al. Tuning the In Vivo Transport of Anticancer Drugs Using Renal-Clearable Gold Nanoparticles. **58**, 8479-8483 (2019).
5. Du, B. et al. Glomerular barrier behaves as an atomically precise bandpass filter in a sub-nanometre regime. *Nature Nanotechnology* **12**, 1096 (2017).